The Cryosphere
Discussions

Modelling the evolution of Djankuat Glacier, North Caucasus, from 1752 until 2100 AD

Yoni Verhaegen[1], Philippe Huybrechts[1], Oleg Rybak[1,2,3] and Victor V. Popovnin[4]

[1]Earth System Science and Department of Geography, Vrije Universiteit Brussel, Pleinlaan 2, B−1050 Brussels, Belgium
5   [2]Water Problems Institute, Russian Academy of Sciences, Gubkina Str. 3,119333 Moscow, Russia
[3]Sochi Research Center, Russian Academy of Sciences, Theatralnaya Str., 8-a, 354000 Sochi, Russia
[4]Department of Geography, Lomonosov Moscow State University, 1 Leninskie Gory, 119991 Moscow, Russia

Correspondence to: Yoni Verhaegen (yoni.verhaegen@vub.be)

10   **Abstract.** We use a numerical 1.5D model to simulate the behaviour of the Djankuat Glacier, a WGMS reference glacier situated in the North Caucasus (Republic of Kabardino-Balkaria, Russian Federation), in response to past, present and future climate conditions (1752−2100 AD). The model consists of a coupled ice flow−mass balance model that also takes into account the evolution of a supraglacial debris cover. After simulation of the past retreat by applying a dynamic calibration procedure, the model was forced with climatic data for the future period under different scenarios regarding temperature, 15   precipitation and debris input. The main results show that the glacier length and surface area have decreased by 1.4 km and 1.6 km² respectively between the initial state in 1752 AD and present-day conditions. Some minor stabilization and/or readvancements of the glacier have occurred, but the general trend shows an almost continuous retreat since the 1850s. Future projections exhibit a further decline of the glacier. Under constant present-day climate conditions, its length and surface area will further shrink by ca. 50 % by 2100 AD. However, even under the most extreme RCP 8.5 scenario, the 20   glacier will not have disappeared completely. The presence of an increasingly widespread supraglacial debris cover is shown to significantly delay glacier retreat, depending on the interaction between the prevailing climatic conditions, the debris input location, the debris mass flux magnitude and the time of release of debris sources from the surrounding topography.

1 Introduction

Recently, a lot of attention has been given to modelling mountain glaciers, in particular due to their worldwide observed 25   shrinkage and important role within the current changing climate. The observed warming trend is a significant matter of concern to scientists and all other people (in)directly involved in the behaviour of these glacial systems, as projected scenarios point towards an even further increase of the global mean temperature in the future, especially if no efficient mitigation strategies are implemented (Vaughan et al., 2013). Being consistent with this global trend, the accelerated retreat of Caucasian glaciers during the last several decades has been clearly noticed (e.g. Shahgedanova et al., 2014; Zemp et al., 30   2015; Tielidze, 2016). Accordingly, total glaciated area has decreased from 691.5 km² to 590.0 km² (-0.52 % yr⁻¹) in the

period between 1986 and 2014 (Tielidze et al., 2017). Further degradation of Caucasian glaciers may affect the supply of water used for drinking, irrigation and hydroelectric energy generation, whereas it may also pose a threat for downstream communities via flooding, glacier collapses, avalanches, debris flows and glacial lake outbursts (e.g. Volodicheva, 2002; Ahouissoussi et al., 2014; Taillant, 2015; Chernomorets et al., 2018). Furthermore, the presence of glaciers in the Caucasus

35 can be considered important for paleoclimatic research, tourism, cultural heritage and biodiversity (e.g. Popovnin, 1999; Shahgedanova et al., 2005; Hagg et al., 2010; Makowska et al., 2016; Tielidze and Wheate, 2018; Rets et al., 2019). Despite these rising concerns, however, modelling of Caucasian glaciers is scarce and has only been attempted in a few studies (e.g. Rybak and Rybak, 2018; Rybak et al., 2018).

In a warming climate, debris cover onto the glacier's surface is believed to increase significantly due to the build-up of more

40 englacial melt-out material., lower flow velocities and increased slope instability, hence favouring the occurrence of rock slides and mass movements from surrounding topography (Østrem, 1959; Kirkbride, 2000; Stokes et al., 2007; Jouvet et al., 2011; Carenzo et al., 2016). Owing to the additional effects of steep terrain, a wet climate, small average glacier size, large lateral moraines and the presence of local easily erodible sedimentary rock outcrops, a sharp increase of debris-covered glacier surfaces has been observed over the Caucasus region. Accordingly, debris coverage has expanded at a rate of ca.

45 +0.32 % yr^{-1} between 1986 and 2014 (Tielidze et al. 2017). Scherler et al. (2018) estimates the supraglacial debris cover on Caucasian glaciers to be 26.2 % at present-day, hence enabling the area to hold the world's most abundant share of debris-covered glacier surfaces in relative terms. Evidently, the presence of such supraglacial debris can influence the evolution of mountain glaciers in a variety of ways, depending on its thickness, properties and spatial/temporal distribution (Nicholson and Benn, 2006; Anderson and Anderson, 2016). More specifically, thick debris has been shown to reduce runoff volumes

50 and reverse mass balance gradients due to its melt-reducing effect (e.g. Østrem, 1959; Bozhinskiy et al., 1986; Anderson and Anderson, 2016). The pronounced effect of debris should therefore not be ignored in numerical experiments to determine the future evolution of mountain glaciers, but, only few studies have included this complex process in time-dependent models, merely using only simple parameterizations (e.g. Jouvet et al., 2011; Rowan et al., 2015; Huss and Fischer, 2016; Kienholz et al., 2017; Rezepkin and Popovnin, 2018).

55 In this paper, we focus on modelling the Djankuat Glacier (North Caucasus, Russian Federation), which has a broad observational network in both space and time. However, despite abundant field data availability and increasing interest concerning future behaviour, the Djankuat Glacier has not yet been modelled extensively. We accordingly present here, for the first time, a 1.5D numerical flow line model for this glacier to simulate its response to past, present and future climatic change. The calculations relate to ice dynamics, supraglacial debris cover evolution and annual surface mass balances. More

60 specifically, the objectives of this study are to construct and calibrate a coupled ice flow−mass balance−supraglacial debris cover model for the Djankuat Glacier, to reconstruct its front variations and mass balance series since 1752 AD, and to simulate the response to future climate change under different scenarios until 2100 AD. In particular, we adapt a more sophisticated and physically based debris model from Anderson and Anderson (2016) to look at the impact of supraglacial

65 debris cover on the glacier's evolution, which has not been previously applied in time-dependent glacier modelling. The results can hence be used to more accurately assess the behaviour of the Djankuat Glacier as representative for the Caucasus area, including the potential side effects of its evolution such as the regulation of water resources. Furthermore, the refined debris cover implementation can be used for comparable glacier models in future research.

2 Location, data and models

2.1 The Djankuat Glacier

70 The Djankuat Glacier [43°12' N, 42°46' E] is a northwest-facing and partly debris-covered temperate valley glacier that is situated on the northern slope of the Main Caucasus Ridge near the border of the Russian Federation and Georgia, which is the most heavily glaciated area of the Northern Caucasus Mountains. It consists of four major ice flows and currently has a length of 3.26 km when taken from its highest point on the south face of the Djantugan peak (Fig. 1). A unique characteristic of the glacier is the origin of its main ice flux on a divergent and vast Djantugan firn plateau south of the main ridge, of
75 which the contributing area to the glacier changes regularly. The Djankuat Glacier has been monitored thoroughly since glaciological measurements began in the 1960s, resulting in an abundant amount of field data and hence enabling this glacier as an ideal candidate for modelling studies (e.g. Popovnin, 1999; Aleynikov et al., 2002; Popovnin and Naruse, 2005; Lavrentiev et al., 2014; WGMS, 2018; Rets et al., 2019). Consequently, the Djankuat Glacier has been selected by the WGMS as a reference glacier for the Caucasus region, hence defining its behaviour as representative for other glaciated
80 areas across the entire Caucasus region. As such, a comparison with glacier length variations in the Caucasus since the 19th century AD shows that the Djankuat Glacier genuinely reflects the general trend in the broader area, as can be seen in Fig. 2 (e.g. Kotlyakov et al., 1991; Solomina et al., 2016; WGMS, 2018).

2.2 Field data

The start of the standard monitoring program on the Djankuat Glacier dates back to 1967/68 AD and includes measurements
85 concerning geometry, supraglacial debris cover and (local) annual surface mass balance. Additionally, ice velocity measurements occurred during the summer seasons of the late 1990s and are based upon both direct (theodolite surveys of stakes) and indirect (stereophotogrammetrical) measurements, of which the resulting maps are reported in Aleynikov et al. (1999) and Pastukhov (2011). Glacier-wide ice thickness maps have also been constructed by Lavrentiev et al. (2014) using ground-based radio-echo measurements. However, direct and reliable observations lack at the higher elevations and the
90 Djantugan Plateau, where ice thickness values have been derived indirectly using surface velocity and slope (Aleynikov et al., 2002; Pastukhov, 2011). As of 2009/10 AD, the glacier occupies a total surface area of 2.688 km², of which the majority is situated at higher elevations (Fig. 3). The current ice thickness goes up to ca. 100 meter in the central part of the main glacier body and to more than 200 meters at the Djantugan Plateau. Moreover, the glacier's cumulative surface mass balance during the 1967/68−2016/17 period exhibits a strongly negative value of -14.33 m w.e. (WGMS, 2018). Both glacier-

95   averaged debris thickness (from 0.28 m in 1983 to 0.54 m in 2010) and total debris-covered area (from ca. 0.10 km² or 3.5 %

in 1968 to ca. 0.34 km² or 12.7 % in 2010) have increased largely. However, at the debris-covered left side of the snout,

debris thickness increased exponentially over the years resulting in mean values of 100 cm at the glacier front in 2010,

compared to 29 cm in 1983 and 45 cm in 1994 AD (Popovnin et al., 2015).

The climate around the glacier can be inferred from nearby weather stations, such as Terskol (elevation 2141 m, approx. 20

100   km northwest of the glacier) and Mestia (approx. 16 km southwest from Djankuat Glacier, in Georgia, at 1441 m elevation),

see Fig. 1. Mean annual temperatures here are +2.8 °C and +6.0 °C respectively for the 1981−2010 period. Especially since

the early 1990s, mean annual temperatures in the area have been increasing, resulting in record high values. Precipitation, on

the other hand, is rather complex due to variations of atmospheric circulation patterns, orographic uplift and convective

precipitation in the summer season (Boyarsky, 1978; Shahgedanova et al., 2007; Hagg et al., 2010; Popovnin and Pylayeva,

105   2015; Rybak et al., 2018). At Terskol and Mestia, total precipitation amounts equal 945.5 and 1035.1 mm yr^{-1} respectively

for the 1981−2010 climate. In the Adylsu Valley (ca. 2650 m elevation) and in the ablation zone of the glacier (ca. 2960 m

elevation), an automatic weather station (AWS) was installed, measuring a wide range of meteorological variables (air

temperature, incoming and outgoing shortwave/longwave radiation, relative humidity and wind speed).

2.3 Ice dynamic model

110   The ice dynamic model is implemented as a 1D (~1.5D) flow line model, in which the prognostic continuity equation for ice

thickness change is solved. We choose to only model ice flow along a central axis in the x-direction and not upgrade the

model to 3D due to the abundant amount of experiments that were conducted. However, the y-dimension is implicitly taken

into account due to inclusion of glacier width along this central axis. As such, one central flow line is considered in the area

with a total length of 5 km, that flows from top to snout and further into the Adylsu Valley (Fig. 1). The flow line was

115   chosen so that it is representative for the Djankuat Glacier as a whole and incorporates the highest point of the glacier near

the Djantugan peak. It remains perpendicular to the surface elevation isolines, while sources of lateral drag near the margins

have a negligible influence on the movement of ice due to its central position. The representativeness was further determined

by ice thickness maps, where the flow line crosses representative areas of thick ice, and dynamical maps, where ice

velocities are large along the major central axis of the glacier. The model treats ice flow as a non-linear diffusion problem in

120   a vertically integrated approach (e.g. Oerlemans, 2001):

$$\frac{\partial H}{\partial t} = -\frac{1}{W_{sfc}}\left(\frac{\partial F_{ice}}{\partial x}\right) + b_a$$

$$= -\frac{1}{W_0 + \mu H}\left[\frac{\partial}{\partial x}\left(\left[(W_0 + \frac{1}{2}\mu H)(\rho_i g H)^3 (f_d H^2 + f_s)\left(\frac{\partial h}{\partial x}\right)^2\right]\frac{\partial h}{\partial x}\right)\right] + b_a, \tag{1}$$

where H is the ice thickness, t the time, μ the slope of the lateral valley walls, W_0 the glacier bed width, W_{sfc} the glacier

surface width, F_{ice} the ice volume flux, x the horizontal distance, b_a the local annual surface mass balance, ρ_i the ice

125 density, g the gravitational acceleration, f_d the flow parameter related to internal deformation, f_s the flow parameter related to basal sliding and h the surface elevation. The vertically integrated velocity is calculated by assuming that the 1D Shallow Ice Approximation is applicable to derive driving stresses on a xz plane and that ice is treated as a homogenous, incompressible and isothermal non-Newtonian fluid in Glen's flow law. For basal sliding, a simplified Weertman-type flow law is used where the basal water pressure is proportional to the ice thickness and the basal shear stress equals the driving

130 stress (e.g. Oerlemans, 1992; Oerlemans, 2001; Leclercq et al. 2012):

$$\overline{u} = \overline{u}_d + u_s = \left(-\rho_i g H \frac{\partial h}{\partial x}\right)^3 \left(f_d H + \frac{f_s}{H}\right), \tag{2}$$

Here, $\overline{u}$ is the vertically averaged horizontal velocity, while $\overline{u}_d$ and u_s are the velocity components related to internal deformation and basal sliding respectively. Equation (1) is then solved on a staggered grid with a spatial resolution Δx of 10 meter starting from zero ice thickness, while the integration over time is achieved with a FTCS scheme using a time step Δt

135 of 0.0005 years. The model was initially run until a steady state situation was reached, which is achieved when the glacier has less than 0.002 % change in its total volume per 25 years.

2.4 Mass balance model

The mass balance model is based upon the trade-off between accumulation ACC and runoff RO over the balance year (1 Oct – 30 Sept), so that the temporal change of the specific surface mass balance b_a is defined as:

140 $$\frac{\partial b_a}{\partial t} = ACC - RO, \tag{3}$$

Mean specific mass balances B_a were calculated as:

$$B_a = \frac{1}{A} \int^A b_a \, dA, \tag{4}$$

where A is the surface area of the glacier. Accumulation is only dependent on the part of the total precipitation that is solid (P_{solid}), which only takes place if precipitation occurs below a certain threshold temperature T_{tresh}:

145 $$ACC = P_{solid} = \begin{cases} ([P_{Terskol} * f_e] * P_{ratio}) * f_{red} & if \ T_{air} < T_{tresh} \\ 0 & if \ T_{air} \geq T_{tresh} \end{cases}, \tag{5}$$

Air temperatures T_{air} from Terskol weather station were interpolated to any surface elevation h on the Djankuat Glacier by applying vertical temperature lapse rates γ_T. Hence, a direct comparison of measured air temperatures between the AWS on Djankuat and the Terskol weather station was found to exhibit a strong correlation (R² = 0.81), generating a summer season lapse rate of -0.0067 °C m^{-1} between 2007−2016 AD. For winter season (Oct−Mar), -0.0049 °C m^{-1} was used in accordance

150 with a mean annual ELA temperature of -3.75 °C for Djankuat Glacier (WGMS, 2018). The term $P_{Terskol} * f_e$ represents the precipitation in the Adylsu Valley, calculated by multiplying the precipitation in Terskol with a horizontal precipitation enhancement factor f_e to account for horizontal precipitation variations. The factor P_{ratio} is used to scale precipitation to the

The Cryosphere
Discussions

entire glacier from the elevation of the Adylsu Valley to any surface elevation h, by making use of a vertical precipitation gradient γ_P. At last, the factor f_{red} represents a snow redistribution factor which corrects the solid precipitation for redistribution by wind and/or avalanches. It was parameterized by dividing the linear accumulation profile with the observed profile and correlating these anomalies to the laterally averaged surface slope s along the flow line (e.g. Huss et al., 2009):

$$f_{red} = \begin{cases} 1.2 & if\ s < s_{crit} \\ -0.0017s^2 + 0.0535s + 0.9041 & if\ s \geq s_{crit} \end{cases}, \tag{6}$$

The critical slope s_{crit} hereby distinguishes between slopes s that either favour snow addition or snow removal. We do acknowledge that the f_{red} parameterization is solely used for curve fitting of the accumulation profile. Melt production M, on the other hand, only takes place when the net energy flux per unit area at the surface Ψ_0 is positive (e.g. Oerlemans, 2001; Nemec et al., 2009):

$$M = max\left(0, \frac{\Psi_0}{\rho_w L_m}\right), \tag{7}$$

where ρ_w is the water density and L_m the latent heat of fusion. This net energy flux is parameterized as (Oerlemans, 2001; Giesen and Oerlemans, 2010; Leclercq et al., 2012):

$$\Psi_0 = \begin{cases} S_\downarrow(1 - \alpha)\tau + c_0 & if\ T_{air} < T_{break} \\ S_\downarrow(1 - \alpha)\tau + c_0 + c_1 T_{air} & if\ T_{air} \geq T_{break} \end{cases}, \tag{8}$$

Here, τ is the atmospheric transmissivity, while c_0 and c_1 are constants to describe the air temperature-dependent fluxes (i.e. the net longwave, latent heat and sensible heat fluxes). The downward incoming solar radiation at the surface $S_\downarrow$ is hereby calculated as (e.g. Oerlemans, 2001):

$$S_\downarrow = \begin{cases} S_{\downarrow(TOA)}(f_{dir}\cos(\theta) + f_{dif}\cos(\theta_z)) & if\ \theta_e > 0° \wedge \theta < 90° \\ S_{\downarrow(TOA)}(f_{dif}\cos(\theta_z)) & if\ \theta_e > 0° \wedge \theta \geq 90° \\ 0 & if\ \theta_e \leq 0° \end{cases}, \tag{9}$$

As such, $S_{\downarrow(TOA)}$ is the incoming instantaneous extraterrestrial shortwave radiation on a horizontal plane at the top of the atmosphere, θ_e and θ_z are the solar elevation and zenith angle respectively and θ is the angle of incidence, which are all calculated using basic astronomical formulas (e.g. Allen et al., 2006; Duffie and Beckman, 2006). Furthermore, f_{dir} and f_{dif} are the fraction of direct and diffuse solar radiation, which are derived from parameterizations used by Oerlemans (1992, 2001, 2010) and Voloshina (2002) that use the fractional cloud cover f_{cl}:

$$\begin{cases} f_{dir} = 0.1 + 0.80(1 - f_{cl}) \\ f_{dif} = 0.9 - 0.80(1 - f_{cl}) \end{cases}, \tag{10}$$

At last, surface albedo α is parameterized as (e.g. Oerlemans and Knap, 1998; Nemec et al., 2009):

$$\alpha = \alpha_{snow} + (\alpha_{ice} - \alpha_{snow})\exp\left(\frac{-d_{snow}}{d^*_{snow}}\right), \tag{11}$$

where α_{snow} is the snow albedo, α_{ice} the ice albedo and d^*_{snow} a characteristic snow depth.

Measurements of the incoming solar radiation from the AWS were used to derive atmospheric transmissivity, which were at

180   first corrected for the tilt at the AWS location (i.e. a slope of 4°). These data were then compared to the theoretical maximum incoming solar radiation at the top of the atmosphere, calculated with standard astronomical formulas (e.g. Allen et al., 2006; Duffie and Beckman, 2006). Consequently, the overall atmospheric transmissivity τ in the summer season over the Djankuat Glacier could be deduced as an average of 0.53 (Table 1). The ice albedo α_{ice} can, according to raw data from the AWS, vary between 0.15 and 0.40 depending on the presence of water, moraine cover and other impurities and has an average

185   value of 0.22, corresponding to moderately debris-loaded ice. Sparse snow-covered conditions during the ablation season causes α_{snow} to increase to the 0.40−0.90 range (mean 0.79). Next, values for f_{dir} and f_{dif} are derived from the parameterization of the fractional cloud cover f_{cl} over the Djankuat Glacier, using the relationship between cloud cover and measured net longwave radiation in the Western Caucasus as found by Voloshina (2002). The analysis points out that direct and diffuse solar radiation are more or less equally important for the glacier (Table 1). The constants c_0, c_1 and T_{break},

190   describing the air-temperature dependent fluxes and their relationship with the air temperature T_{air} itself, are derived from measurements of the AWS of the net longwave radiation, as well as from a parameterization of the sensible and latent heat fluxes via Kuzmin's method (Kuzmin, 1961; Toropov et al., 2017). Here, these fluxes are added up and plotted against air temperature following the method of Giesen and Oerlemans (2010) and Leclercq et al. (2012), as can be seen from Eq. (8).

2.5 Debris cover model

195   The supraglacial debris cover on the Djankuat Glacier was parameterized in order to account for the effects of melt reduction under debris-covered ice. The debris thickness was approached with a steady deposit model adopted from Anderson and Anderson (2016), where debris input onto the glacier is generated from a fixed point on the flow line. In the model, debris thickness then changes according to either melt-out from debris-loaded ice (first term), the downstream advection of supraglacial debris (second term) and the input or removal of supraglacial debris on the glacier surface (third term):

200    $$\frac{\partial H_{debris}}{\partial t} = -\left(\frac{C_{debris}(\min(0,b_a))}{(1-\phi_{debris})\rho_{debris}}\right) - \left(\frac{\partial(u_{sfc}H_{debris})}{\partial x}\right) + I_{debris}, \tag{12}$$

Here, H_{debris} is the debris thickness, t the time, C_{debris} the englacial debris concentration, ϕ_{debris} the debris cover porosity, ρ_{debris} the debris rock density, b_a the specific surface mass balance, u_{sfc} the glacier surface velocity and I_{debris} the input or removal of debris from the glacier surface. In the model, the factors ϕ_{debris} and ρ_{debris} are constants in space and time and taken at 0.43 and 2600 kg m^{-3} respectively (Bozhinskiy et al., 1986). For C_{debris}, we use a value of 1.05 kg m^{-3}, referring to

205   the value of 0.12 % as found by the same authors for the Djankuat Glacier in the 1980s (Table 1).

At the debris input location x_{debris}, a steady debris flux per unit area F^{input}_{debris} transmits material from the surrounding topography to the glacier by means of a debris deposition rate (m yr^{-1}), starting from the time of release of the debris source t_{debris} onwards. We set the debris input location at 1680 m from the highest point, since it is the furthest point up-glacier for

which observed debris thickness values are reported in Popovnin et al. (2015). To avoid the buildup of unrealistically high

210 debris thickness in low flow velocity zones in the future period, we choose to let the debris mass flux stop when the surface

width at point x_{debris} has reached a value lower than 90 % ($t_{Wsfc-10\%}$) of its original value at time t_{debris}. This is a

reasonable value, as the current observed debris-covered area is ca. 10 % at this specific point (Fig. 3). Consequently, by

then the glacier has shrunk too much to ensure proper connectivity between the debris source and the glacier surface. At the

terminus (the last non-zero ice thickness grid point), debris is removed into the foreland by a debris flux per unit area $F_{debris}^{x=T}$

215 (Anderson and Anderson, 2016):

$$
I_{debris} = \begin{cases} F_{debris}^{input} & if \; x = x_{debris} \wedge t_{debris} \leq t < t_{Wsfc-10\%} \\ -F_{debris}^{x=T} = c_T H_{debris}^{x=T} & if \; x = x_T \\ F_{debris}^{x=T+1} = F_{debris}^{x=T(orig)} - F_{debris}^{x=T} & if \; x = x_{T+1} \\ 0 & else \end{cases} \tag{13}
$$

where x_T is the terminus position and c_T is a constant describing the strength of debris removal from the terminus into the

foreland, for which we used the same value as suggested in Anderson and Anderson (2016), i.e. $c_T = 1$ (Table 1). As such,

what is deposited in the foreland by $F_{debris}^{x=T+1}$ is the difference between the original debris flux on point $x = x_T$ (i.e. without

220 the parameterization) minus the actual debris flux obtained with the parameterization. The advection equation is solved using

a first order upwind scheme with $\Delta t = 0.01$ years. Eventually, the debris-related melt reduction factor f_{debris} is taken as

(e.g. Vacco et al., 2010; Huss and Fischer, 2016):

$$
f_{debris} = \exp\left(\frac{-H_{debris}}{H_{debris}^*}\right), \tag{14}
$$

Here, H_{debris}^* is a characteristic debris thickness. Next, the fractional debris covered area along the flow line is parameterized

225 based upon the distance from the terminus D_T, for which a relationship was found from observations and can, of course, not

exceed 1:

$$
\frac{A_{debris}}{A} = \min(G_A \exp(-0.01612 * D_T - 0.01720), 1), \tag{15}
$$

Here, G_A is a yearly updated growth factor that controls the expansion of the debris covered area. As such, in the case that

snow is present at the glacier surface, runoff is calculated as the meltwater outflow from a saturated snowpack W_{snow},

230 following the principles applied in Schaefli and Huss (2011). On the other hand, in case of snow-free conditions, runoff is

affected by the presence of a debris cover on the glacier ice (e.g. Lambrecht et al., 2011):

$$
RO = \begin{cases} W_{snow} = max(0, w_{snow} - \eta_s d_{snow}) & if \; d_{snow} > 0 \\ M_{ice} = M\left(\frac{A-A_{debris}}{A}\right) + M\left(\frac{A_{debris}}{A}\right)f_{debris} & if \; d_{snow} = 0 \end{cases}, \tag{16}
$$

where M is the melt production (see Sect. 2.4), W_{snow} is the water outflow from the saturated snowpack, w_{snow} the liquid

snow store, η_s the water holding capacity of the snowpack, f_{debris} the melt-reduction factor from debris, A_{debris} the debris

235 covered area and d_{snow} the snow depth.

3 Model setup and calibration

3.1 Mass balance model

We used the 1967/68−2006/07 period to calibrate the mass balance model, as this time frame holds both specific (elevation-dependent) and mean specific (glacier-wide) surface mass balance measurements (WGMS, 2018). Accordingly, temperature and precipitation data of the corresponding period were used from the Terskol and Mestia weather stations. For geometric data that serve as input for solar geometry calculations, we use laterally averaged values for slope and aspect, calculated by averaging all intra-glacier values along a line perpendicular to the flow line. Surface elevations were directly extracted from a DEM for 2009/10 AD conditions. We hereby take into account the same spatial spacing of 10 m that is used in the flow model. Afterwards, geometric input data were smoothed using a window size of ± 100 m around every grid point. Calibration of the mass balance model further assumes the geometry (slope, aspect, glacier length and surface area) to be fixed over this time period, whereas in fact length and surface area decreased by 113 m and 0.346 km^2 respectively.

For the accumulation part, the precipitation enhancement factor f_e and the vertical precipitation gradient γ_P were used as tuning parameters. In literature, horizontal precipitation enhancement factors varying between 1.2 and 1.7 have been proposed between Terskol and the Adylsu Valley to account for horizontal precipitation variation in the area, whereas several vertical precipitation gradients have been proposed as well, varying between 0.0005 and 0.0046 m yr^{-1} m^{-1} (e.g. Boyarsky, 1978; Hagg et al., 2010; Giesen and Oerlemans, 2012; WGMS, 2018; Rybak et al., 2018). To ensure successful calibration, a precipitation enhancement factor of 1.5 between Terskol and the Adylsu Valley was found to be sufficient, whereas a precipitation gradient of 0.0023 m w.e. yr^{-1} m^{-1} was derived to extract these data over the entire glacier surface. At last, the snow redistribution factor f_{red} was used for curve fitting of the accumulation profile, as discussed before.

Concerning ablation, three variables were chosen as tuning parameters. Due to lack of field data concerning the water holding capacity of snow η_s, it was used to calibrate the ablation in the accumulation area. For the factor H^*_{debris}, which controls the strength of the melt reducing effect of debris, values between 0.18 and ±0.60 m have been proposed for Djankuat Glacier (Bozhinskiy et al., 1986; Lambrecht et al., 2011). According to Rybak (2018), on the other hand, melt-reduction factors f_{debris} around 0.35−0.45 are modelled near the terminus, implying a value for H^*_{debris} of ±0.95−1.25 m. Due to the large uncertainty regarding this factor, it was used as second a tuning parameter, this time for the lower elevation areas. Additionally, the intercept of the air temperature-dependent fluxes c_0 was chosen as a final tuning parameter due to the lack of reliable and/or sufficient data below T_{break} during the observational period (Table 1).

With the calibrated surface energy balance model, the multiyear mean mass balance profile of the Djankuat Glacier during the 1967/68–2006/07 period is successfully reproduced, as the mass balance vs. elevation profile matches nicely with its observed counterpart (Fig. 4). This profile reflects the determinative processes affecting the Djankuat Glacier's mass

balance: in the higher elevations, snow redistribution by wind/avalanches and meltwater retention are important factors, whereas in the lower areas, the presence of a supraglacial debris cover reduces glacier's runoff volume significantly and hence dampens the mass balance gradient. Modelled mean specific balances of the Djankuat Glacier show a moderate
270 agreement with observed values since 1967/68 AD (R^2 = 0.52). The RMSE of the individual local annual mass balances and the multiyear mean mass balance-elevation profile was reduced to 0.61 m w.e. yr^{-1} m^{-1} (R^2 = 0.91) and 0.18 m w.e. yr^{-1} m^{-1} (R^2 = 0.99) respectively (Fig. 4).

3.2 Debris cover model

For the debris model calibration, we matched the temporal evolution of the average debris thickness at the front (i.e. the first
275 30 grid points) as well as the debris covered area, using t_{debris}, F_{debris}^{input} and G_A as tuning parameters. Values for the observed debris cover at different elevation bands from the survey year 1968 AD (only for debris area) as well as for 1983, 1994 and 2010 AD (for both debris area and thickness) are therefore available from Popovnin et al. (2015). Moreover, to obtain more detailed information concerning the current debris covered area on a spatial scale, the debris cover extent was manually digitized based on satellite imagery of the year 2010 (see Fig. 1).

280 Accordingly, the observed debris thickness evolution was found to be best reproduced by setting t_{debris} to 1958 and F_{debris}^{input} to 1.60 m yr^{-1} (Table 1). At last, a power relation (R^2 = 0.85) was found between the growth factor G_A and the modelled mean debris thickness at the glacier front as obtained in the previous step

$$G_A = 1.17048 * \left(H_{debris}^{front}\right)^{0.62047},$$ (17)

Where H_{debris}^{front} is the modelled debris thickness at the front (i.e. the first 30 grid points) as obtained before. As such, the
285 RMSE between modelled and observed values between 1967/68 and 2009/10 AD was reduced to 0.07 m (R^2 = 0.83) for debris thickness at the front and 0.9 % (R^2 = 0.95) for the fractional debris-covered area respectively (Fig. 5).

3.3 Ice dynamics model

To calibrate the flow model, the parameters f_d and f_s were adopted to minimize the RMSE between observed and modelled ice thickness for 2009/10 AD conditions, hereby assuming a steady state. Geometric input data for the flow model were
290 therefore extracted from a DEM for 2009/10 AD conditions. Hence, bedrock elevation was derived in combination with ice thickness maps from Pastukhov (2011) and Lavrentiev et al. (2014). Surface width was extracted by measuring the intra-glacier distance of 10-meter spaced lines perpendicular to the orientation of the flow line. After extracting the lateral valley slopes, the width at the bed was calculated, where a trapezoidal valley shape was assumed (e.g. Oerlemans, 1992; Gantayat et al., 2017). All data were finally joined to the closest point on the flow line for every 10 m and smoothed with a window of
295 ± 100 m around every grid point.

For the Djankuat Glacier, the best fit was found for $f_d = 6.5 \times 10^{-17}$ Pa^{-3} yr^{-1} and $f_s = 3.25 \times 10^{-13}$ Pa^{-3} m^2 yr^{-1} (Table 1). Additionally, the bed width was slightly adjusted to ensure that the area-elevation distribution and the total surface area of 2.688 km^2 fit well with observed values. The full set of parameter values used in the model is given in Table 1.

The flow model for the Djankuat Glacier was able to produce a steady state glacier profile with a length of 3.26 km after 200
300 years (Fig. 6). The model approaches the observed ice thickness as it minimizes the RMSE to 14.27 m (R² = 0.90). Despite minimized RMSE, the mismatch near the snout and steep slopes near the Djantugan peak increase the error of the model. However, it is argued that a significant part of the error reflects either the current non-steady state situation of the glacier and the presence of a supraglacial debris cover at the front, or the lack of reliable and direct ice thickness observations at the highest elevations of the glacier. Modelled current surface velocity for the Djankuat Glacier goes up to 79.7 m yr^{-1} near the
305 ice falls of the Djantugan Plateau and also peak in the middle section of the glacier, which fits well with observations of maximum velocities in the 60−80 m yr^{-1} range (Aleynikov et al., 1999; Pastukhov, 2011). Moreover, the modelled deformational and basal sliding components comprise respectively 45 % and 55 % of the vertically averaged ice flow velocity along the flow line.

4 Basic sensitivity experiments

310 Sensitivity experiments show that the mass balance of the Djankuat Glacier, when geometry and other parameters are considered fixed, is quite sensitive to both temperature (-0.70 m yr^{-1} w.e. °C^{-1}) and precipitation changes (+0.20 m yr^{-1} w.e. 10 %$^{-1}$). As such, a 1 °C annual temperature change for the Djankuat Glacier is only compensated when the precipitation change is in the order of ca. 35 %, although mass balance sensitivity to temperature changes shows a non-linear behaviour whereas the relationship is linear for precipitation changes (Fig. 7). Also mass balance sensitivity to atmospheric
315 transmissivity and albedo (combined for snow and ice) is large, as these values are calculated to -0.25 m yr^{-1} w.e. (0.05)$^{-1}$ and +0.57 m yr^{-1} w.e. (0.05)$^{-1}$ respectively. The latter shows a slightly non-linear trend, where sensitivity changes more drastically for negative mass balances compared to positive values. Forcing the flow model with a mass balance profile in the case of debris-free conditions shows that the steady state glacier length would be 310 m (ca. 10 %) smaller than current values, at 2940 m.

320 Especially in the 2700−2800 m ASL zone, reduction of runoff related to supraglacial debris increased significantly, as values rise from ca. 3 % reduction before the 1970s to ca. 40 % by 2009/10 AD (Fig. 8). By 2010 AD, the debris-related melt reduction factor f_{debris} has decreased towards ca. 0.45 in this area, while fractional debris covered area increased to nearly 100 %. In the 2800−2900 m ASL zone, runoff reduction increased from ca. 1 % to ca. 17 %, while in the 2900−300 m ASL zone values increased from ca. 0.5 % to 7 % reduction during that same period. The glacier-wide runoff was not affected
325 significantly before the 1970s (< 1 %) but was reduced by ca. 9 % around 2009/10 AD geometry (glacier-wide runoff volume decreases from ca. 3.81 to ca. 3.42 million m³ around 2009/10 AD) when compared to debris-free conditions with identical glacier. As such, the presence of supraglacial debris causes the local mass balance of the Djankuat Glacier to be ca.

11

23 %, 9 % and 4 % higher, on average over the calibration period, in the 2700−2800, 2800−2900 and 2900−3000 m ASL zones respectively. The effect is, however, not significantly pronounced further up-glacier.

330   Sensitivity experiments with the flow model show a linear relationship between the steady state glacier front position and mass balance perturbations. As such, the steady state glacier length varies with 1280 m (m yr^{-1} w.e.)$^{-1}$. On the other hand, the e-folding length response time of Djankuat is in the order of 31±3 years (Fig. 9). Response times seems to be slightly shorter for negative perturbations, which can be related to the steeper upslope terrain, increasing mass balance gradient in a warming climate and a smaller glacier size (Oerlemans, 2001). Sensitivity of steady state glacier length to temperature

335   changes is modelled to be 815 m °C^{-1}, while for precipitation the corresponding value is 250 m 10 %$^{-1}$. For atmospheric transmissivity and surface albedo, the steady state length sensitivity comprises values of 300 m (0.05)$^{-1}$ and 650 m (0.05)$^{-1}$. A temperature increase of +3.4 °C compared to the 1967/68−2006/07 Terskol mean of +2.5 °C is sufficient to cause a total drawdown of the glacier, as the last ice on the Djantugan Plateau melts away 470 years after the induced perturbation.

5 Past reconstruction of the Djankuat Glacier

340   ### 5.1 LIA extent of the glacier

All three submodels (ice flow, mass balance and debris cover) are finally coupled to determine the past and future evolution of the Djankuat Glacier. Here, the mass balance model and debris cover model calculate annual surface mass balance profiles, which are then used as input for the continuity equation in the ice flow model but converted to ice equivalents. Glacier length L is hereby calculated by counting up all non-zero ice thickness grid points multiplied by Δx. L is thus not

345   necessarily equal to the glacier terminus position.

As a first step, the model is initialized with a spin up run in which a steady state glacier, as well as a steady state debris cover, are produced for the balance year 1752/53 AD. Although we have no clear indication to suspect steady state behaviour at this time due to lack of reliable debris cover, mass balance and length change data, it was imposed to start the simulations without unwanted transient model drift at the initial stage. Hence, we choose to let the glacier grow until the

350   length indicated by the end moraine of the 18th century (4.62 km), which has been determined by lichenometric dating in the paleovalley (Boyarsky, 1978; Zolotarev, 1998; Petrakov et al., 2012), see Fig. 1. For debris cover, we assume that only melt out processes add debris to the glacier, which implies that debris mass fluxes from surrounding topography are not incorporated in the initialization procedure. To obtain a steady state glacier, the multiyear mean mass balance profile for the 1967/68−2006/07 climate had to be perturbated with an additional ΔB_a of +1.12 m yr^{-1} w.e., corresponding to an ELA

355   lowering of 113 m. The steady state situation of the model was then tested by comparing the ice flux with the integrated upstream mass balance, by ensuring that the surface mass balance over the entire glacier equals 0 to within an acceptable accuracy and by calculating the volume change with time. As expected for the model setup, all results exhibited an appropriate steady state situation for the glacier.

It can be noted that modelled ice thickness around the maximum extent of the glacier in the considered model period went up
360 to 173.4 m in the valley. Additionally, surface velocities were as high as 101.7 m yr^{-1} near the ice falls of the Djantugan
Plateau and up to 98.1 m yr^{-1} in the valley downstream (Fig. 6).

5.2 Evolution of the glacier from 1752 AD to present

To force the model, climatic data at 3-hourly intervals were needed. Historic climatic datasets for Terskol weather station
were therefore constructed using information from various weather stations in the area, including Mestia, Pyatigorsk
365 (approximately 100 km northeast from the glacier at 512 m elevation) and Mineralnye Vody (approximately 115 km
northeast from the glacier at 321 m elevation). Additionally, historic data from the CRUTEM4 and CRU TS datasets, as well
as from tree ring reconstructions for the broader Caucasus area, were used for the remaining uncovered data gaps since 1752
AD (D'Arrigo et al., 2001; Toucham et al., 2003; Akkemik et al., 2005; Akkemik and Aras, 2005; Griggs et al., 2007; Köse
et al., 2011; Jones et al., 2012; Harris et al., 2014; Holobâcă et al., 2015; Martin-Benito et al., 2016; Dolgova, 2016). At first,
370 data from for the pre-observational period outside the Terskol time series (1977−2013 with a data gap between 1990−1997)
were averaged on a yearly basis over all the available datasets, both for precipitation and temperature. Next, mean monthly
temperatures and precipitation amounts were derived by matching the mean and standard deviation of the overlapping parts
of the obtained dataset with those from Terskol weather station (Table 2). To obtain a record with a 3-hourly temporal
resolution, the data sequence for Terskol over which measurements with a 3-hourly interval are available (1977−2013 with a
375 data gap between 1990−1997) is repeated into the past and future in order to maintain intra-daily and intra-annual variability
in the data. These data were afterwards corrected for the monthly mean temperature and precipitation amounts obtained in
the previous step (Table 2).

The reconstruction of temperature and precipitation clearly indicates a shift in the climatic conditions after 1752 AD.
Especially during the last two decades, an accelerated warming trend has occurred, as temperatures have been increasing at
380 an unprecedented rate. For temperature, a clear sequence of colder and warmer intervals can be seen, as clearly colder
periods in the dataset are noticeable around the 1770−80s, 1830−40s, 1860s, 1880s, late 1890s into the early 1900s, late
1910s, early 1930s, early 1940s and during the 1970−80s AD. Warmer intervals, on the other hand, have occurred during the
1750−60s, 1790−1800s, 1820s, 1850s, 1870s, early 1890s, 1920s, late 1930s, 1950−60s and during the last two decades. The
latest 30-year mean climatic interval of 1988−2017 exhibits a mean annual temperature anomaly of +0.72 °C compared to
385 the 1961−1990 mean, making it the warmest period in the whole time series. Wetter periods have occurred during the early
1850s, 1870−80s, late 1890s into the early 1900s, late 1910s and early 1920s, late 1930s into early 1940s and early 2000s.
Drier periods were present during the 1860s, early 1890s, late 1900s into the early 1910s, late 1920s, late 1940s and 1990s
(Fig. 10).

After using the steady state glacier of 1752/53 AD as an initial input feature for the time-dependent model, dynamic
390 calibration is applied by iteratively adding additional mass balance perturbations to the obtained mass balance profile that

13

was simulated with the climatic input, until the reconstructed glacier length matched with the observed values over the years (e.g. Oerlemans, 1997; Zekollari et al., 2014). The dynamic calibration procedure required a maximum additional mass balance perturbation of +0.5 m w.e. yr^{-1}. Nevertheless, since the balance year 1967/68 AD, i.e. the year from which the mass balance model was calibrated, no additional perturbations were needed. It can thus be stated that the model performs well

395 and underwent a successful validation to within acceptable accuracy.

The resulting mass balance series shows clear peaks around the 1870−80s, early 1900s, late 1910s, 1940s, 1970s and early 2000s AD, hereby coinciding with slightly colder and/or wetter periods in the climatic datasets (Fig. 11). Clear minima in the mass balance series can be noted in the 1860s, 1890s, early 1910s, 1920s, late 1940s and in the 21th century, which agrees fairly well with earlier mass balance reconstructions of Djankuat (Dyurgerov and Popovnin, 1988; Fyodorov and Zalikhanov, 2018) and Garabashi glaciers on the Elbrus massif (Rototaeva et al., 2003; Dolgova et al., 2013). As the

400 Djankuat Glacier reacted to these climatic perturbations, an almost continuous retreat since the 1850s AD has been pursued, exhibiting some minor readvances or steady states as well. As was already discussed earlier, the past behaviour of the Djankuat Glacier is in line with the general observed trend for other Caucasian glaciers (Fig. 2). During the last several decades, however, the addition of a thickening layer of supraglacial debris on the snout aided to temporarily postpone rapid

405 retreat and more or less maintain steady state conditions. Still, the glacier has lost a total length of 1.39 km at present-day compared to the start of the reconstruction in 1752 AD. The reconstruction also shows that the total glacier area around 1752 AD was about 54 % larger compared to the 2009/10 AD situation, with an area of 4.147 against 2.688 km^2 (Fig. 6 and 11). Moreover, evolution of glacier surface area matches nicely with observed values except for the outlier around 1983, which has to do with a migrating ice divide on the Djantugan Plateau (Fig. 11).

410 **6 Future glacier evolution to 2100 AD**

Future projections of temperature and precipitation (2019−2100 AD) were obtained by using output of the CMIP5 simulations for the country of Georgia under 4 different RCP scenarios (Alder and Hostetler, 2013). Hence, to force the model into the future, we use the RCP 2.6, RCP 4.5, RCP 6.0 and RCP 8.5 scenarios. As such, mean temperature and precipitation were changed linearly on a yearly basis, until the 2071−2095 AD mean values matched the CMIP5 simulation

415 output for the different scenarios. All scenarios exhibit a further increase of the mean annual temperature, as well as a decreasing precipitation amount compared to the reference climate (Table 3). The most extreme changes, however, exist in the RCP 8.5 scenario, as Terskol mean annual temperatures increase to +7.1 °C by 2071−2095 AD. Additionally, also a future projection will be made under a no change scenario, in which the current climate (2007−2016 AD) is repeated with respect to its mean until 2100 AD.

420 Concerning debris cover evolution, the debris input location x_{debris} and flux magnitude F_{debris}^{input} were left unchanged. Consequently, once the contribution from x_{debris} stops, either due to shrinkage of the surface width or rapid retreat beyond the input location, no additional debris source is released. Hence, only melt out from debris-loaded ice and supraglacial

debris advection contribute to the evolution of the supraglacial debris cover. Later on, we have, however, conducted several experiments to determine the impact of potential additional debris sources from the surrounding topography on the future

425   glacier evolution.

All future scenarios agree to a rapid decline of the glacier length and surface area in the following decade, as a response to the significant warming since the late 1990s AD (Fig. 12). The experiments also show that, even for the no change scenario, the glacier will shrink drastically. By 2100 AD, the total length and surface area of the glacier are projected to be 1640 m (-50 %) and 1.275 km² (-53 %), whereas the glacier front will be positioned at an elevation of 3131 m in that scenario. It is

430   thus clear that, at present day, the Djankuat Glacier is not in equilibrium with the current climatic conditions and hence will strive towards a new steady state with a much smaller surface area in the future. For the RCP 2.6, 4.5, 6.0 and 8.5 scenarios, the total glacier length further decreases to 1250 m (-62 %), 1020 m (-69 %), 930 m (-72 %) and 680 m (-79 %) by 2100 AD respectively. Meanwhile, total glacier surface area decreases to 0.760 km² (-72 %), 0.423 km² (-84 %), 0.372 km² (-86 %) and 0.139 km² (-95 %) by 2100 AD respectively (Fig. 12). As such, for the RCP 6.0 and 8.5 scenarios, the glacier

435   retreats back as far as into the bedrock depression of the Djantugan Plateau.

With respect to total runoff volume changes and water resources management, the Djankuat Glacier has already surpassed its peak water discharge point, as the modelled annual glacier runoff has reached its maximum around 2010 AD (Fig. 13). Hence, all RCP scenarios exhibit a further decline of the produced runoff volume into the future, which is in accordance with earlier work for this area (Huss & Hock, 2018; SROCC, 2019). The actual course of runoff changes, however, is dependent

440   upon the trade-off between remaining glacier surface area and magnitude of melt. As such, the RCP 8.5 scenario initially produces the highest melt and corresponding runoff volume. Later on, however, the 'no change' scenario yields the highest runoff volumes due to the larger remaining glaciated area. It must also be noted that near the end of the modelling period, runoff volume increases again for the RCP 6.0 and RCP 8.5 scenarios. This process is related to the melting of the ice on the Djantugan Plateau, which then reinforces itself due to the mass balance-elevation feedback.

445   However, even under the most extreme RCP 8.5 scenario, the glacier would not completely disappear by the end of the modelling period. Despite accelerated melting of the high-elevation plateau because of the mass balance-elevation feedback, a decreased climate sensitivity due to the steeper laterally averaged slopes in the upper glacier part, as well as the large ice thickness on the Djantugan Plateau (up to 200 meter at present-day), prevent a complete disappearance by the end of the modelling period.

450   **7 Impact of supraglacial debris cover on glacier evolution**

Debris input onto the Djankuat Glacier's surface due to mass fluxes from surrounding topography are expected to increase even further in the future (Popovnin et al., 2015; Rezepkin and Popovnin, 2018). To determine the potential effect of these additional debris sources onto the glacier surface, we executed some experiments with varying debris input location, debris input magnitude and time of the release of the debris source from the surrounding topography. We repeated the procedure

The Cryosphere
Discussions

455   used in Sect. 2.5, but indicated a 'debris reference scenario', in which a second debris mass flux is initiated from $x_{debris} = $ 1000 meter at $t_{debris} = 2035$ with a magnitude of $F_{debris}^{input} = 1.5$ m yr^{-1}. We then let one of these three variables change, while keeping the other two at their original value of the 'reference situation'. As such, the debris input location x_{debris} was changed to 1250, 1500 and 1750 m, the time of release t_{debris} to 2050, 2065 and 2080, and at last the magnitude of the debris flux F_{debris}^{input} to 2.0, 2.5 and 3.0 m yr^{-1} (Fig. 14).

460   The effect of the timing of the source release is straightforward: the earlier the debris mass flux is released, the larger the extension of the glacier by the year 2100 AD, as the melt-reducing effect starts earlier in time. The main decisive factor here is the efficient debris advection towards the terminus, because flow velocities are larger in 2035 AD compared to 2050, 2065 and 2080 AD (Fig. 14). The magnitude of the debris input flux F_{debris}^{input} is another crucial parameter determining the length extension of the Djankuat Glacier in the future period. It is, hence, obvious that a higher flux magnitude will contribute more

465   efficiently to a higher debris growth rate. This enhanced effect is a direct consequence of the implementation of Eq. (14), where the debris-related melt reduction depends on the debris thickness (Fig. 14). Concerning the debris input location, results suggest that the closer the input source is located to the terminus, the longer the extension of the glacier will be compared to the situation without an additional debris source. This makes sense, as the time that it takes for the supraglacial debris to be advected to the front is shorter for down-glacier input locations. Hence, the debris cover will be able to apply its

470   melt-reducing effect much earlier in time, as well as much further down-glacier in space on a still relatively long glacier.

    The effect of climatic conditions on debris-related melt reduction and its impact on glacier geometry is twofold. Initially, the melt-reducing effect increases with higher temperature, as can be seen in the case of the no change, RCP 2.6 and RCP 4.5 scenarios. This can be related to the fact that a higher temperature will increase the melt-out of material from debris-loaded ice, whereas also decreased flow velocities prevent sufficient discharge and allow the debris to thicken quickly up-glacier.

475   Moreover, the distances between the input point and the glacier front at the time of source release decrease with increasing temperature, whereas also retreat rates are relatively larger for higher temperatures. This allows the relatively thick debris to encounter the glacier front much earlier in time. At last, it is important to note that for the same melt reduction factor f_{debris}, the absolute reduction of the ablation amount will be higher when the initial value of the ablation is high. However, for the RCP 6.0 and RCP 8.5 scenarios, the impact of the supraglacial debris cover on the glacier decreases again. Here, a

480   counteracting effect occurs as temperatures rise even further, because the risk of rapid loss of debris-covered area increases. This can be related to either the breaking of the glacier into several fragments where areas of 'dead ice' prevent proper connectivity between the main glacier body and the glacier front, or because the front is too close to (or has already passed) the debris source by the time it is released. Finally, the accelerated shrinkage also favours foreland deposition instead of debris accumulation due to frontal retreat, as well as the loss of proper connectivity between the debris source and the main

485   glacier body at the debris input location (Eq. 13, Fig. 14).

8 Conclusion

In this study, a coupled ice flow−mass balance−supraglacial debris cover model was used to simulate the response of the Djankuat Glacier to past, present and future climatic changes between 1752 and 2100 AD. We conducted, for the first time, explicit time-dependent modelling of a Caucasian glacier, including an extended and physically based subroutine related to

490 supraglacial debris cover evolution that was not yet integrated in previous glaciological models. As it turns out, the Djankuat Glacier has been retreating almost continuously since the 1850s AD, with some minor steady states or readvances during periods with clusters of colder and/or wetter conditions. The model reconstructed the observed retreat fairly well but required additional mass balance perturbations up to a maximum of +0.5 m yr^{-1} w.e., which were applied iteratively via dynamic calibration. However, since the start of the calibration period in the balance year 1967/68 AD, no artificial mass balance

495 perturbations were needed, ensuring proper model validation.

Future behaviour of the glacier will be determined by corresponding changes in air temperature, precipitation and supraglacial debris cover. A temperature increase of 1 °C can only be compensated by a precipitation increase of ca. 35 %, which is not indicated by future climatic projections in the study area. Hence, all scenarios agree to a rapid decline during the following decade, as a response to the accelerating warming since the 1990s AD. Even after considering constant present-

500 day climatic conditions, the glacier will shrink drastically to ca. 50 % of its current length and surface area by 2100 AD, indicating the imbalance between the current glacier geometry and the present climate. However, none of the future scenarios cause a total disappearance by the end of the modelling period. Nevertheless, the glacier will retreat most drastically (ca. -80 %) under the RCP 8.5 scenario, as even the thick ice on the high elevations of the Djantugan Plateau will be affected by significant melting. Although the glacier has already surpassed its peak water discharge point, the modelled

505 temporal evolution of total runoff volumes indicates that, in particular the melting of ice on these higher parts of the glacier in higher-temperature scenarios, re-intensifies runoff near the end of the modelling period due to the mass balance-elevation feedback.

The presence of a supraglacial debris cover is shown to significantly affect glacier geometry during the modelling period. Hence, the effect of debris-related melt reduction on the eventual glacier length by 2100 AD is dependent upon the trade-off

510 between the growth rate of the total supraglacial debris mass, the efficiency of down-glacier advection of supraglacial debris, the glacier retreat rate, the connectivity between the debris source and the main glacier, and finally the distance between the front and the input location at the time of source release. It turns out that debris-related effects are highest when either debris thickness and area are large, or when melt-reducing effects start earlier in time and/or more down-glacier in space in a relatively warm climate. However, it must be noted that for some of the conducted experiments, the addition of an extra

515 debris source did not (significantly) influence the glacier's geometry. As such, when temperatures increase even further, potential inhibiting effects of too rapid shrinkage are to be considered. Hence, accelerated frontal retreat, disrupted debris discharge and/or connectivity issues at the debris input location may prevent the establishment of a proper melt-reducing effect.

The Cryosphere
Discussions

Open Access

EGU

520

Code availability. The model code was written in MATLAB_R2019a and is available from Y.V. on request.

Data availability. The reconstructed historic and future climatic datasets for the Terskol meteo station are available from Y.V. on request.

525

Author contribution. Y.V. created the climatic datasets, constructed and calibrated the numerical model, performed the numerical simulations and wrote the manuscript. P.H. proposed the main conceptual ideas and outlines, helped design and implement the research, provided guidance in interpreting the results and improved the manuscript throughout the entire process. O.R. and V.V.P. contributed by making glacier field work possible, providing numerous datasets and improving the

530   manuscript with their knowledge and years of experience concerning the Djankuat Glacier.

Competing interests. The authors declare that they have no conflict of interest.

References

Ahouissoussi, N., Neumann, J. E., Srivastava, J. P., Okan, C., and Droogers, P. (Eds.): Reducing the vulnerability of

540   Georgia's agricultural systems to climate change: impact assessment and adaptation options, World Bank Publications, Georgia, 116 pp., 2014.

Akkemik, Ü, Dagdeviren, N., and Aras, A.: A preliminary reconstruction (A.D. 1635–2000) of spring precipitation using oak tree rings in the western Black Sea region of Turkey, Int. J. Biometeorol., 49(5), 297–302, doi: 10.1007/s00484−004−0249−8, 2005.

545   Akkemik, Ü., and Aras, A.: Reconstruction (1689–1994 AD) of April–August precipitation in the southern part of central Turkey, Int. J. Climatol., 25(4), 537–548, doi: 10.1002/joc.1145, 2005.

Alder, J. R., and Hostetler, S. W.: An interactive web application for visualizing climate data, Eos Trans. AGU, 94(22), 197–198, doi: 10.1002/2013EO220001, 2013.

Aleynikov, A. A., Popovnin, V. V., Voytkovskiy K. F., and Zolotaryov Y. A.: Indirect estimation of the Djankuat Glacier
550   volume based on surface topography, Hydrol. Res., 33(1), 95−110, doi: 10.2166/nh.2002.0006, 2002.

Aleynikov, A. A., Zolotarev, E. A., and Popovnin, V. V.: The velocity field of Djankuat Glacier [Поле скоростей ледника
Джанкуат], Data of Glaciological Studies, 87(1), 169−176, 1999 [in Russian].

Allen, R. G., Trezza, R., and Tasumi, M.: Analytical integrated functions for daily solar radiation on slopes, Agric For
Meteorol., 139 (1–2), 55–73, doi: 10.1016/j.agrformet.2006.05.012, 2006.

555   Anderson, L. S., and Anderson, R. S.: Modeling debris-covered glaciers: response to steady debris deposition, The
Cryosphere, 10(1), 1105−1124, doi: 10.5194/tc−10−1105−2016, 2016.

Boyarsky, I.Y.: The Djankuat Glacier [Ледник Джанкуат] (Ed. by I.Y. Boyarsky), Gidrometeoizdat, Leningrad, USSR, 184
p., 1978 [in Russian].

Bozhinskiy, A. N., Krass, M. S., and Popovnin, V. V.: Role of debris cover in the thermal physics of glaciers, J. Glaciol.,
560   32(111), 255–266, doi: 10.3189/S0022143000015598, 1986.

Carenzo, M., Pellicciotti, F., Mabillard, J., Reid, T., and Brock, B.W.: An enhanced temperature index model for debris-
covered glaciers accounting for thickness effect, Adv. Water Resour., 94(1), 457–469, doi: 10.1016/j.advwatres.2016.05.001,
2016.

Chernomorets, S. S., Petrakov, D. A., Aleynikov, A. A., Bekkiev, M. Y., Viskhadzhieva, K. S., Dokukin, M. D., Kalov, R.
565   K., Kidyaeva, V. M., Krylenko, V. V., Krylenko, I. V., Krylenko, I. N., Rets, E. P., Savernyuk, E. A., and Smirnov, A. M.:
The outburst of Bashkara glacier lake (central Caucasus, Russia) on september 1, 2017 [Прорыв озера Башкара
(Центральный Кавказ, Россия) 1 сентября 2017 года], Earth's Cryosphere, 22(2), 70–80, doi:
0.21782/EC2541−9994−2018−2(61−70), 2018 [in Russian].

D'Arrigo, R., and Cullen, H. M.: A 350-year (AD 1628–1980) reconstruction of Turkish precipitation, Dendrochronologia,
570   19(2), 169–177, 2001.

Dolgova, E.: June–September temperature reconstruction in the Northern Caucasus based on blue intensity data,
Dendrochronologia, 39(1), 17–23, doi: 10.1016/j.dendro.2016.03.002, 2016.

Dolgova, E. A., Matkovsky, V. V., Solomina, O. N., Rototaeva, O. V., Nosenko, G. A., and Khmelevskoy, I. F.:
Reconstruction of the mass balance of the Garabashi glacier (1800–2005) using dendrochronological data [Реконструкция
575   баланса массы ледника Гарабаши (1800–2005 гг.) по дендрохронологическим данным], Ice and Snow, 1(121), 34–41,
doi: 10.15356/2076−6734−2013−1−34−42, 2013 [in Russian].

Duffie, J. A., and Beckman, W. A.: Solar thermal energy processes, Wiley Interscience, New York, 944 p., 2006.

19

Dyurgerov, M. B., and Popovnin, V. V.: Reconstruction of mass balance, spatial position, and liquid discharge of Dzhankuat Glacier since the second half of the 19th century, Data of glaciological studies, 40(1), 111–126, 1988 [Russian Translations Series 67].

580

Fyodorov, V. M., and Zalikhanov, A. M.: Analysis of changes in the ice resources of the Central Caucasus [Анализ изменения ледовых ресурсов Центрального Кавказа], Proc. T.I.Vyazemskiy Karadag Res. Station, RAS nature reserve [Труды Карадагской научной станции им. Т.И. Вяземского-природного заповедника РАН], 3(7), 68–83, 2018 [in Russian].

585 Gantayat, P., Kulkarni, A. V., Srinivasan, J., and Schmeits, M. J.: Numerical modelling of past retreat and future evolution of Chhota Shigri glacier in Western Indian Himalaya, Ann. Glaciol., 58(75pt2), 136−144, doi: 10.1017/aog.2017.21, 2017.

Giesen, R. H., and Oerlemans, J.: Response of the ice cap Hardangerjøkulen in southern Norway to the 20th and 21st century climates, The Cryosphere, 4(1), 191–213, doi: 10.5194/tc−4−191−2010, 2010.

Giesen, R. H., and Oerlemans, J.: Calibration of a surface mass balance model for global-scale applications, The Cryosphere, 590 6(6), 1463–1481, doi: 10.5194/tc−6−1463−2012, 2012.

Griggs, C., De Gaetano, A., Kuniholm, P., and Newton, M.: A regional high-frequency reconstruction of May–June precipitation in the north Aegean from oak tree rings, A.D. 1089–1989, Int. J. Climatol., 27(8), 1075–1089, doi: 10.1002/joc.1459, 2007.

Hagg, W., Shahgedanova, M., Mayer, C., Lambrecht, A., and Popovnin, V. V.: A sensitivity study for water availability in 595 the Northern Caucasus based on climate projections, Glob. Planet. Change, 73(1), 161–171, doi: 10.1016/j.gloplacha.2010.05.005, 2010.

Harris, I., Jones, P., Osborn, T., and Lister, D.: Updated high-resolution grids of monthly climatic observations—The CRU TS3.10 Dataset, Int. J. Climatol., 34(3), 623–642, doi: 10.1002/joc.3711, 2014.

Holobâcă, I. H., Pop, O., and Petrea, D.: Dendroclimatic reconstruction of late summer temperatures from upper treeline 600 sites in Greater Caucasus, Russia, Quat. Int., 415(3), 67–73, doi: 10.1016/j.quaint.2015.10.103, 2016.

Huss, M., Bauder, A., and Funk, M.: Homogenization of long-term mass-balance time series, Ann. Glaciol., 50(50), 198–206, doi: 10.3189/172756409787769627, 2009.

Huss, M., and Fischer, M.: Sensitivity of very small glaciers in the Swiss Alps to future climate change, Front. Earth Sci., 40(34), 1–17, doi: 10.3389/feart.2016.00034, 2016.

605 Huss, M., and Hock, R.: Global-scale hydrological response to future glacier mass loss, Nat. Clim. Change, 8(2). 135–140, doi: 10.1038/s41558-017-0049-x, 2018.

Jones, P. D., Lister, D. H., Osborn, T. J., Harpham, C., Salmon, M., and Morice C. P.: Hemispheric and largescale land surface air temperature variations: an extensive revision and an update to 2010, J. Geophys. Res., 117(D05), 1–29, doi: 10.1029/2011JD017139, 2012.

610 Jouvet, G., Huss, M., Funk, M., and Blatter, H.: Modelling the retreat of Grosser Aletschgletscher, Switzerland, in a changing climate, J. Glaciol., 57(206), 1033–1045, doi: 0.3189/002214311798843359, 2011.

Kienholz, C., Hock, R., Truffer, M., Bieniek, P. A., and Lader, R.: Mass balance evolution of Black Rapids glacier, Alaska, 1980–2100, and its implications for surge recurrence, Front. Earth Sci., 5(56), 1–20, doi: 10.3389/feart.2017.00056, 2017.

Kirkbride, M. P.: Ice-marginal geomorphology and Holocene expansion of debris-covered Tasman Glacier, New Zealand.
615 Debris-Covered Glaciers (Proceedings of a workshop held at Seattle, Washington, USA, September 2000), 264(1), 211–217, doi: 10.1007/978−90−481−2642−2_622, 2000.

Köse, N., Akkemik, Ü., Dalfes, H.N., and Özeren, M. S.: Tree-ring reconstructions of May–June precipitation for western Anatolia, Quat. Res., 75(3), 438–450, doi: 10.1016/j.yqres.2010.12.005, 2011.

Kotlyakov, V. M., Serebryanny, R. L., and Solomina, O. N: Climate change and glacier fluctuation during the last 1,000
620 years in the Southern Mountains of the USSR, Mt. Res. Dev., 11(1), 1–12, 1991.

Kuzmin, P. P.: The processes of Snow Cover Melting, Gidrometeoizdat, Leningrad, USSR. 348 p., 1961 [translated from Russian by E. Vilim].

Lambrecht, A., Mayer, C., Hagg, W., Popovnin, V. V., Rezepkin, A., Lomidze, N., and Svanadze, D.: A comparison of glacier melt on debris-covered glaciers in the northern and southern Caucasus, The Cryosphere, 5(1), 525–538, doi:
625 10.5194/tc−5−525−2011, 2011.

Lavrentiev, I. I., Kutuzov S. S., Petrakov, D. A., Popov, G. A., and Popovnin, V. V.: Ice thickness, volume and subglacial relief of Djankuat Glacier (Central Caucasus) [Толщина, объём льда и подлёдный рельеф ледника Джанкуат (Центральный Кавказ)], Ice and Snow, 4(128), 7–19, doi: 10.15356/2076−6734−2014−4−7−19, 2014 [in Russian].

Leclercq, P. W., Pitte, P., Giesen, R. H., Masiokas, M. H., and Oerlemans, J.: Modeling and climatic interpretation of the
630 length fluctuations of Glacier Frias (north Patagonian Andes, Argentina) 1639−2009 AD, Clim. Past., 8(1), 1385–1402, doi: 10.5194/cp−8−1385−2012, 2012.

Makowska, N., Zawierucha, K., Mokracka, J., and Koczura, R.: First report of microorganisms of Caucasus glaciers (Georgia), Biol., 71(6), 620–625, doi: 10.1515/biolog−2016−0086, 2016.

Martin-Benito, D., Ummenhofer C. C., Köse, N., Güner, H. T., and Pederson, N.: Tree-ring reconstructed May−June
635 precipitation in the Caucasus since 1752 CE, Clim. Dyn., 47(9–10), 3011–3027, doi: 10.1007/s00382−016−3010−1, 2016.

The Cryosphere
Discussions

EGU Open Access

Nemec, J., Huybrechts, P., Rybak, O., and Oerlemans, J.: Reconstruction of the annual balance of Vadret da Morteratsch, Switzerland, since 1865, Ann. Glaciol., 50(50), 126–134, doi: 10.3189/172756409787769609, 2009.

Nicholson, L., and Benn, D. I.: Calculating ice melt beneath a debris layer using meteorological data, J. Glaciol., 52(178), 463–470, doi: 10.3189/172756506781828584, 2006.

640 Oerlemans, J., and Knap, W. H.: A 1-year record of global radiation and albedo in the ablation zone of Morteratschgletscher, Switzerland, J. Glaciol., 44(147), 231–238, doi: 10.3189/S0022143000002574, 1998.

Oerlemans, J.: Climate sensitivity of glaciers in southern Norway: application of an energy-balance model to Nigardsbreen, Hellstugubreen and Ålfotbreen, J. Glaciol., 38(129), 223–232, doi: 10.3189/S0022143000003634, 1992.

Oerlemans, J.: A flowline model for Nigardsbreen, Norway: projection of future glacier length based on dynamic calibration
645 with the historic record, Ann. Glaciol., 24(1), 382–389, doi: 10.3189/S0260305500012489, 1997.

Oerlemans, J.: Glaciers and climate change, A. A. Balkema Publishers, Lisse, 160 pp., 2001.

Oerlemans, J.: The microclimate of valley glaciers, Utrecht Publishing and Archiving Services, Utrechtm, 138 pp., 2010.

Østrem, G.: Ice melting under a thin layer of moraine, and the existence of ice cores in moraine ridges, Geogr. Ann., 41(4), 228– 230, 1959.

650 Pastukhov, V. G.: On the mass exchange of the Djankuat Glacier [Полный массообмен ледника Джанкуат], Graduate work, Moscow State University (Faculty of Geography), 185 pp., 2011 [in Russian].

Petrakov, D. A., Tutubalina, O. V., Aleynikov, A. A., Chernomorets, S. S., Evans, S. G., Kidyaeva, V. M., Krylenko, I. N., Norin, S. V., Shakhmina, M. S., and Seynova, I. B.: Monitoring of Bashkara Glacier lakes (Central Caucasus, Russia) and modelling of their potential outburst, Nat. Hazards, 61(3), 1293–1316, doi: 10.1007/s11069−011−9983−5, 2012.

655 Popovnin, V. V., Rezepkin, A. A., and Tielidze, L. G.: Superficial moraine expansion on the Djankuat glacier snout over the direct glaciological monitoring period [Разрастание поверхностной морены на языке ледника Джанкуат за период прямого гляциологического мониторинга], Earth's Cryosphere, 19(1), 79–87, 2015 [in Russian].

Popovnin, V. V., and Naruse, R.: A 34-year long record of mass balance and geometric changes of the Djankuat Glacier, Caucasus, Bull. Glaciol. Res., 22(1), 121–133, 2005.

660 Popovnin, V. V., and Pylayeva T. V.: Avalanche feeding of Djankuat Glacier [Лавинное питание ледника Джанкуат], Ice and snow, 55(2), 21–32, doi: 10.15356/2076−6734−2015−2−21−32, 2015 [in Russian].

Popovnin, V. V.: Annual mass-balance series of a temperate glacier in the Caucasus, reconstructed from an ice core, Geogr. Ann. Ser. A-phys. Geogr., 81(4), 713–724, doi: 10.1111/1468−0459.00099, 1999.

665 Rets, E. P., Popovnin, V. V., Toropov, P. A., Smirnov, A. M., Tokarev, I. V., Chizhova, J.N., Budantseva, N.A., Vasil'chuk, Y.K., Kireeva, M.B., Ekaykin., A.A., Veres, A.N., Aleynikov, A.A., Frolova, N.L., Tsyplenkov, A.S., Poliukhov, A.A., Chalov, S.R., Aleshina, M.A. and Kornilova, E.D.: Djankuat Glacier station in the North Caucasus, Russia: a database of complex glaciological, hydrological, meteorological observations and stable isotopes sampling results during 2007−2017, Earth Syst. Sci. Data, 11, 1463–1481, doi: 10.5194/essd-11-1463-2019, 2019.

670 Rezepkin, A. A., and Popovnin, V. V.: Influence of the surface moraine on the state of Djankuat Glacier (Central Caucasus) by 2025 [О влиянии поверхностной морены на состояние ледника Джанкуат (Центральный Кавказ) к 2025 г.], Ice and snow, 58(3), 307–321, doi: 10.15356/2076−6734−2018−3−307−321, 2018 [in Russian].

Rototaeva, O. V., Nosenko, G. A., Khmelevskoy, I. F., and Tarasova, L. N.: Balance state of the Garabashi glacier (Elbrus) in 1980-s and 1990-s [Состояние равновесия ледника Гарабаши (Эльбрус) в 1980-х и 1990-х годах], Data of Glaciological Studies, 95(1), 111–121, 2003 [in Russian].

675 Rowan, A. V., Egholm, D. L., Quincey, D. J., and Glasser, N. F.: Modelling the feedbacks between mass balance, ice flow and debris transport to predict the response to climate change of debris covered glaciers in the Himalaya, Earth Planet. Sci. Lett., 430(1), 427–438, doi: 10.1016/j.epsl.2015.09.004, 2015.

Rybak, O. O., Rybak, E. A., Korneva, I. A., and Popovnin, V. V.: Mathematical modelling of Djankuat Glacier evolution in present-day climatic conditions, Sustainable Dev. of Mt. Territories, 10(4), 533–543, doi: 680 10.21177/1998−4502−2018−10−4−533−543, 2018.

Rybak, O., and Rybak, E. A.: Model-based calculations of surface mass balance of mountain glaciers for the purpose of water consumption planning: focus on Djankuat Glacier (Central Caucasus), IOP Conference Series: Environ. Earth Sci., 107(1), 1–7, doi: 10.1088/1755−1315/107/1/012041, 2018.

Schaefli, B., and Huss, M.: Integrating point glacier mass balance observations into hydrologic model identification, Hydrol. 685 Earth Syst. Sci., 15(1), 1227–1241, doi: 10.5194/hess−15−1227−2011, 2011.

Scherler, D., Wulf, H., and Gorelick, N.: Global Assessment of Supraglacial Debris Cover Extents, Geophys. Res. Lett., 45(21), 11798–11805, doi: 10.1029/2018GL080158, 2018.

Shahgedanova, M., Nosenko, G., Kutuzov, S., Rototaeva, O., and Khromova, T.: Deglaciation of the Caucasus Mountains, Russia/Georgia, in the 21st century observed with ASTER satellite imagery and aerial photography, The Cryosphere, 8(1), 690 2367–2379, doi: 10.5194/tc−8−2367−2014, 2014.

Shahgedanova, M., Popovnin, V. V., Aleynikov, A. A., Petrakov, D., and Stokes, C. R.: Long-term change, inter-annual, and intra-seasonal variability in climate and glacier mass balance in the Central Greater Caucasus, Russia, Ann. Glaciol., 46(1), 355–361, doi: 10.3189/172756407782871323, 2007.

Shahgedanova, M., Stokes, C. R., Gurney, S. D., and Popovnin, V. V.: Interactions between mass balance, atmospheric
695   circulation and recent climate change on the Djankuat Glacier, Caucasus Mountains, Russia, J. Geophys. Res. Atmos..
110(D4), 1–14, doi: 10.1029/2004JD005213, 2005.

Solomina, O., Bushueva, I., Dolgova, E., Jomelli, V., Alexandrin, M., Mikhalenko, V., and Matskovsky, V.: Glacier
variations in the Northern Caucasus compared to climatic reconstructions over the past millennium, Glob. Planet. Change,
140(1), 28–58, doi: 10.1016/j.gloplacha.2016.02.008, 2016.

700   SROCC: Chapter 2: High Mountain Areas. In: IPCC Special Report on the Ocean and Cryosphere in a Changing Climate
[H.-O. Pörtner, D.C. Roberts, V. Masson-Delmotte, P. Zhai, M. Tignor, E. Poloczanska, K. Mintenbeck, M. Nicolai, A.
Okem, J. Petzold, B. Rama, N. Weyer (eds.)], 2019.

Stokes, C. R., Popovnin, V. V., Aleynikov, A. A., Gurney, S. D., and Shahgedanova, M.: Recent glacier retreat in the
Caucasus Mountains, Russia, and associated increase in supraglacial debris cover and supra-/proglacial lake development,
705   Ann. Glaciol., 46(1), 195−203, doi: 10.3189/172756407782871468, 2007.

Taillant, J. D.: Glaciers: the politics of ice, Oxford University Press, Oxford, 360 pp., 2015.

Tielidze, L. G.: Glacier change over the last century, Caucasus Mountains, Georgia, observed from old topographical maps,
Landsat and ASTER satellite imagery, The Cryosphere, 10(1), 713–725, doi: 10.5194/tc−10−713−2016, 2016.

Tielidze, L., and Wheate, R.: The Greater Caucasus Glacier Inventory (Russia, Georgia and Azerbaijan), The Cryosphere,
710   12(1), 81–94, doi: 10.5194/tc−12−81−2018, 2018.

Tielidze, L. G., Wheate, R. D., Kutuzov, S. S., Doyle, K., and Lavrentiev, I. I.: Supraglacial debris cover assessment in the
Caucasus Mountains, 1986−2000−2014, Earth Syst. Sci. Data, 96(1), 1–21, doi: 10.5194/essd−2017−96, 2017.

Toropov P. A., Shestakova, A., and Smirnov, A. M.: Methodological aspects of heat balance components estimation on
mountain glaciers, Russ. J. Earth Sci., 17(4), 1–9, doi: 10.2205/2017ES000605, 2017.

715   Toropov, P. A., Aleshina, M. A., Kislov, A. V., and Semenov, V. A.: Trends of climate change in the Black sea-Caspian
region in the last 30 years [Тенденции изменений климата Черноморско-Каспийского региона за последние 30 лет].
Moscow University Herald, Geogr. Ser., 5(2), 67–77, 2018 [In Russian].

Toucham, R., Garfin, G. M., Meko, D. M., Funkhouser, G., Erkan, N., Hughes, M. K., and Wallin, B. S.: Preliminary
reconstructions of spring precipitation in southwestern Turkey from tree-ring width, Int. J. Climatol., 23(2), 157–171, doi:
720   10.1002/joc.850, 2003.

Vacco, D. A., Alley, R. B., and Pollard, D.: Glacier advance and stagnation caused by rock avalanches, Earth Planet. Sc.
Lett., 294(1), 123–130, doi: 10.1016/j.epsl.2010.03.019, 2010.

Vaughan, D. G., Comiso, J., Allison, I., Carrasco, J., Kaser, G., Kwok, R., ... et al.: Observations: Cryosphere. In T. F. Stocker, D. Qin, G. K. Plattner, M. Tignor, S. K. Allen, J. Boschung, A. Nauels, ... et al. (Eds.), Climate change 2013: The

725   physical science basis. Contribution of working group I to the fifth assessment report of the intergovernmental panel on climate change Cambridge, United Kingdom and New York, NY, USA: Cambridge University Press, 317–382, 2013.

Volodicheva, N.: The Caucasus [edited by: Shahgedanova, M.], in: The Physical Geography of Northern Eurasia, Oxford University Press, 350–376, 2002.

Voloshina, A. P.: Meteorology of mountain glaciers [Метеорология горных ледников], Data of Glaciological Studies,

730   92(1), 3–138, 2002 [In Russian].

WGMS: Djankuat, North Caucasus. [World Glacier Monitoring Service ONLINE]. Available at: https://wgms.ch/products_ref_glaciers/djankuat/, last access: 17 December 2019, 2019.

Zekollari, H., Fürst, J., and Huybrechts, P.: Modelling the evolution of Vadret da Morteratsch (Switzerland) since the Little Ice Age and into the future, J. Glaciol., 60(224), 1155–1168, doi: 10.3189/2014JoG14J053, 2014.

735   Zemp, M., Frey, H., Gärtner-Roer, I., Nussbaumer, S., Hoelzle, M., Paul, F., … et al.: Historically unprecedented global glacier decline in the early 21st century, J. Glaciol., 61(228), 745–762. doi: doi.org/10.3189/2015JoG15J017, 2015.

Zolotarev, E. A.: About the "moraine of the 30s" and the size of the Dzhankuat glacier [О конечной "морене 30-х годов" и размерах ледника Джанкуат], Data of Glaciological Studies, 87(1), 177–183, 1998 [in Russian].

740

745
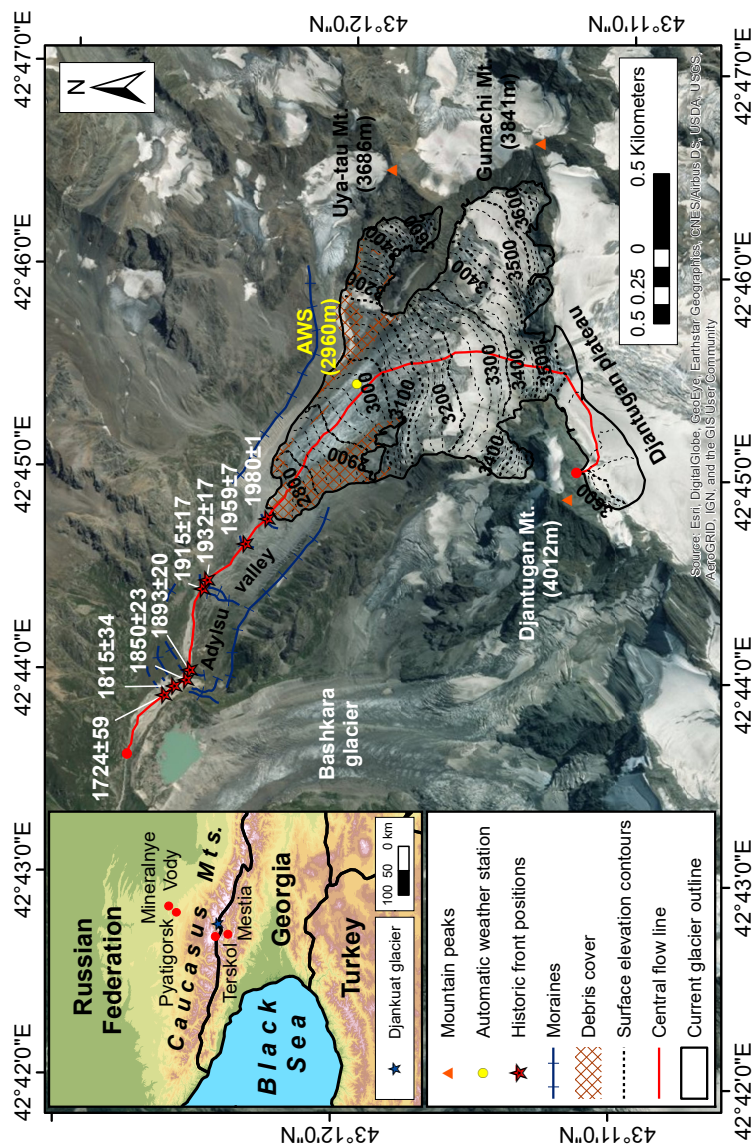
Figure 1. Satellite image of the Djankuat Glacier for the year 2010 AD, showing the most important features in the study area.
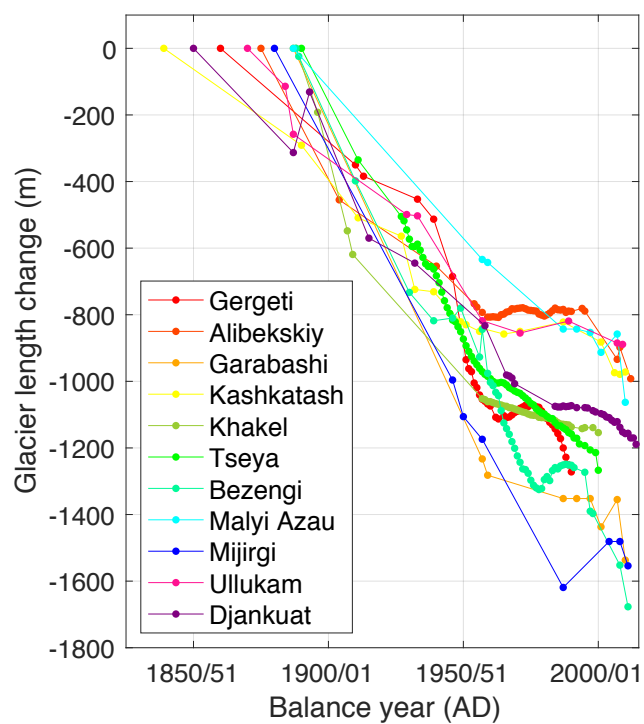
Figure 2. Comparison of modelled historic length variations of the Djankuat Glacier to other glaciers in the Caucasus area. Observed length variations are derived from Solomina et al. (2016) and WGMS (2018).
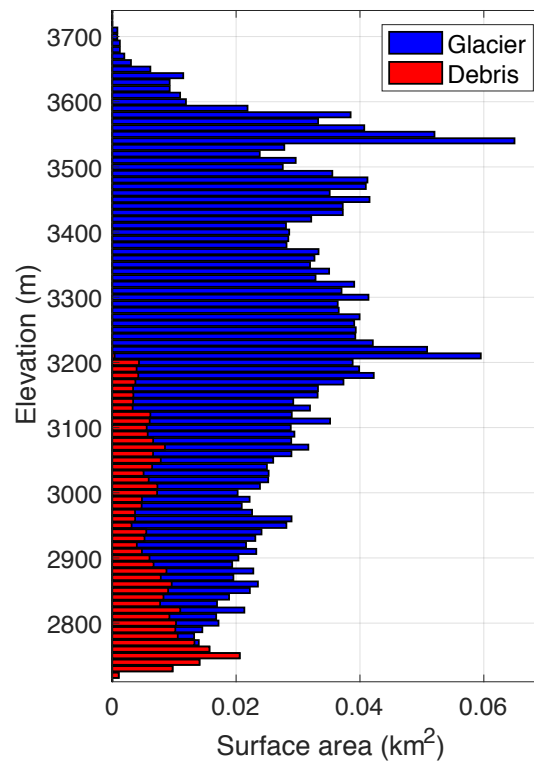
755

Figure 3. The Djankuat Glacier's surface (blue) and debris covered area (red) for 2009/10 AD conditions as shown by the area-elevation distribution using 10-meter bins. Hypsometric data are derived from the DEM and manual digitalization of the supraglacial debris cover using satellite imagery in Fig. 1.
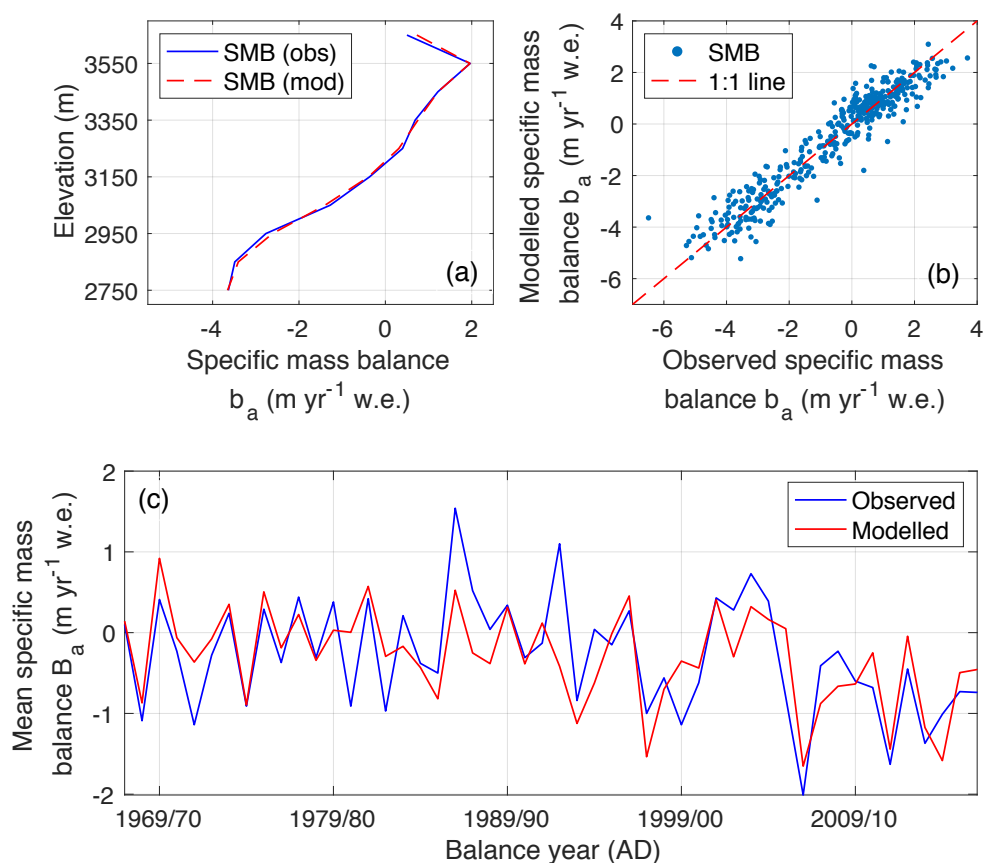
The Cryosphere
Discussions

760

Figure 4. Calibrated mass balance model of the Djankuat Glacier for fixed geometry, showing the observed and modelled (a) mass balance-elevation profile for the 1967/68−2006/07 period, (b) local annual surface mass balances b_a for the 1967/68−2006/07 period and (c) modelled and observed mean specific mass balance B_a since the start of the monitoring period until present. Observed mass balance data are retrieved from Popovnin & Naruse (2005) and WGMS (2018).

765
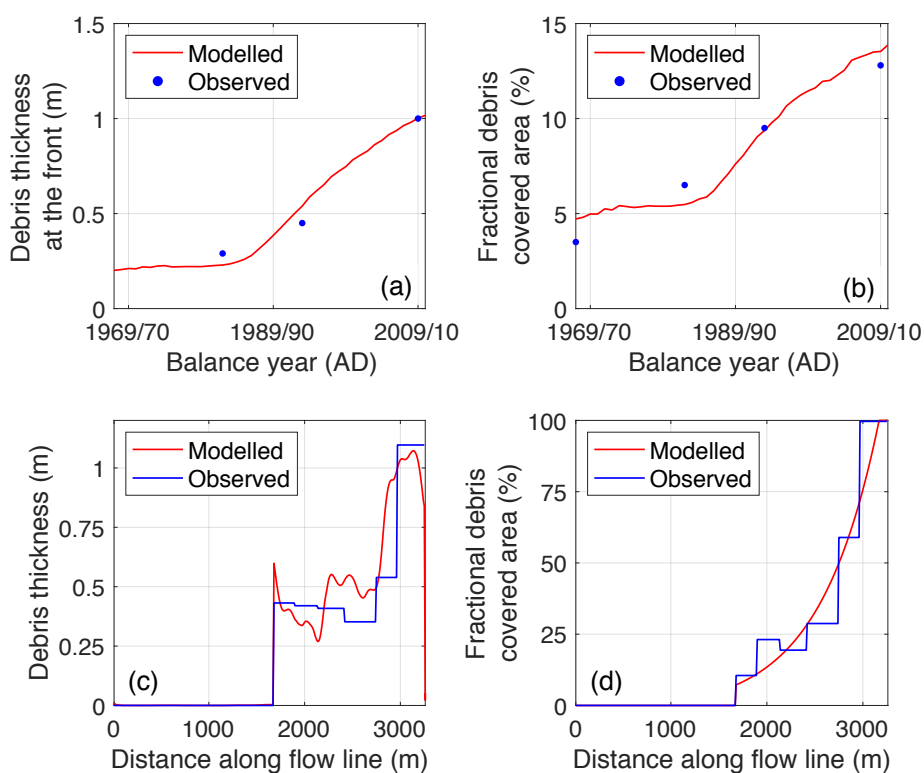
Figure 5. Calibrated supraglacial debris cover model for the Djankuat Glacier, showing the observed and modelled temporal evolution of (a) debris thickness at the front and (b) the glacier-wide fractional debris covered area, as well as observed and modelled (c) debris thickness and (d) debris covered area along the flow line for 2009/10 AD conditions. Observed data from (a), (b) and (c) are from Popovnin et al. (2015), whereas the observed debris covered area in (d) was derived by manually digitizing debris-covered patches along the flow line using 2010 AD satellite imagery in Fig. 1.
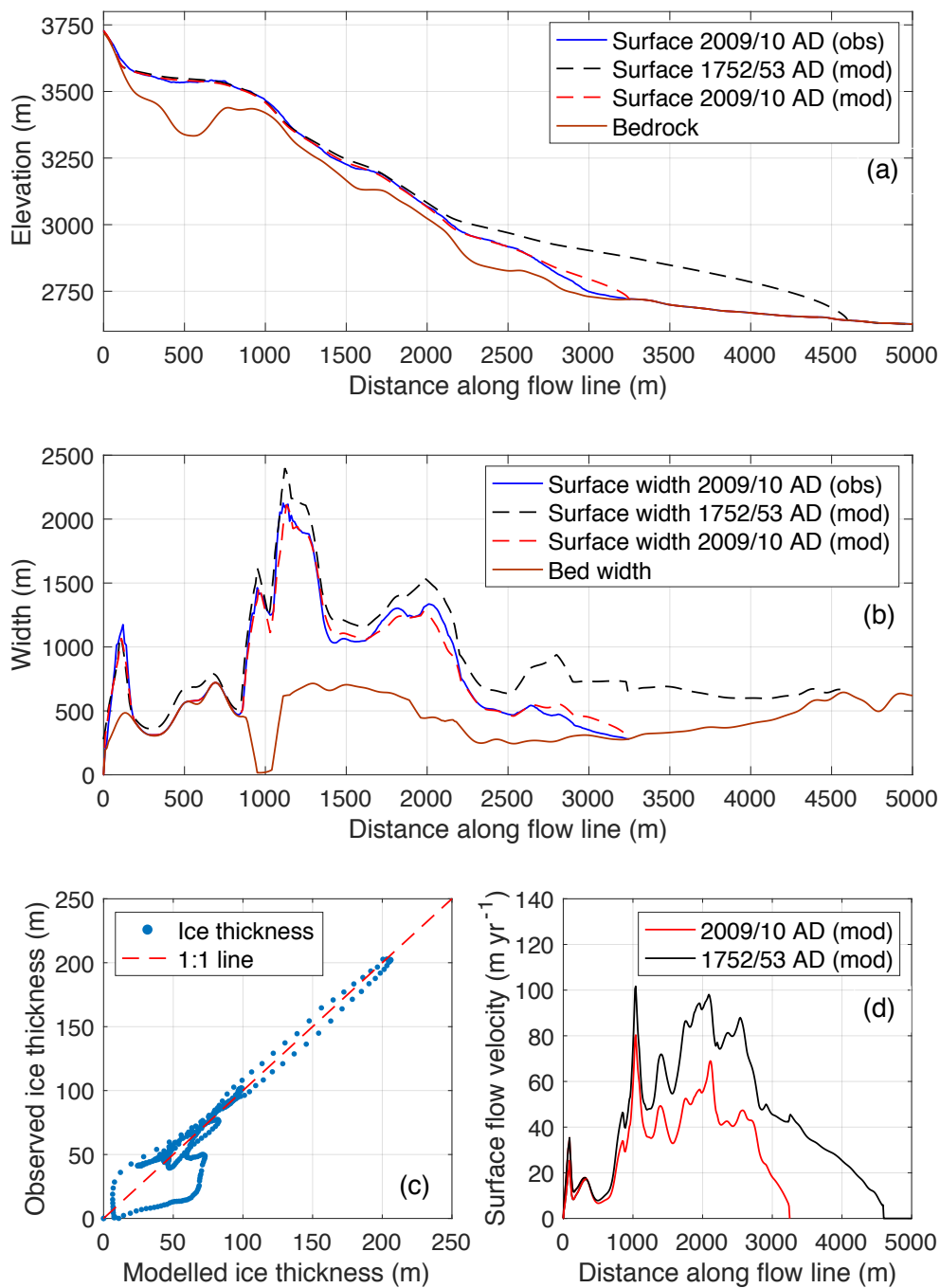
Figure 6. Calibrated flow model, showing (a) the observed and modelled bedrock and surface elevation and (b) bed and surface width for the current (2009/10 AD) and initial state (1752/53 AD), (c) modelled vs. observed ice thickness for 2009/10 AD conditions and (d) current (2009/10 AD) and initial (1752/53 AD) surface flow velocity along the flow line.
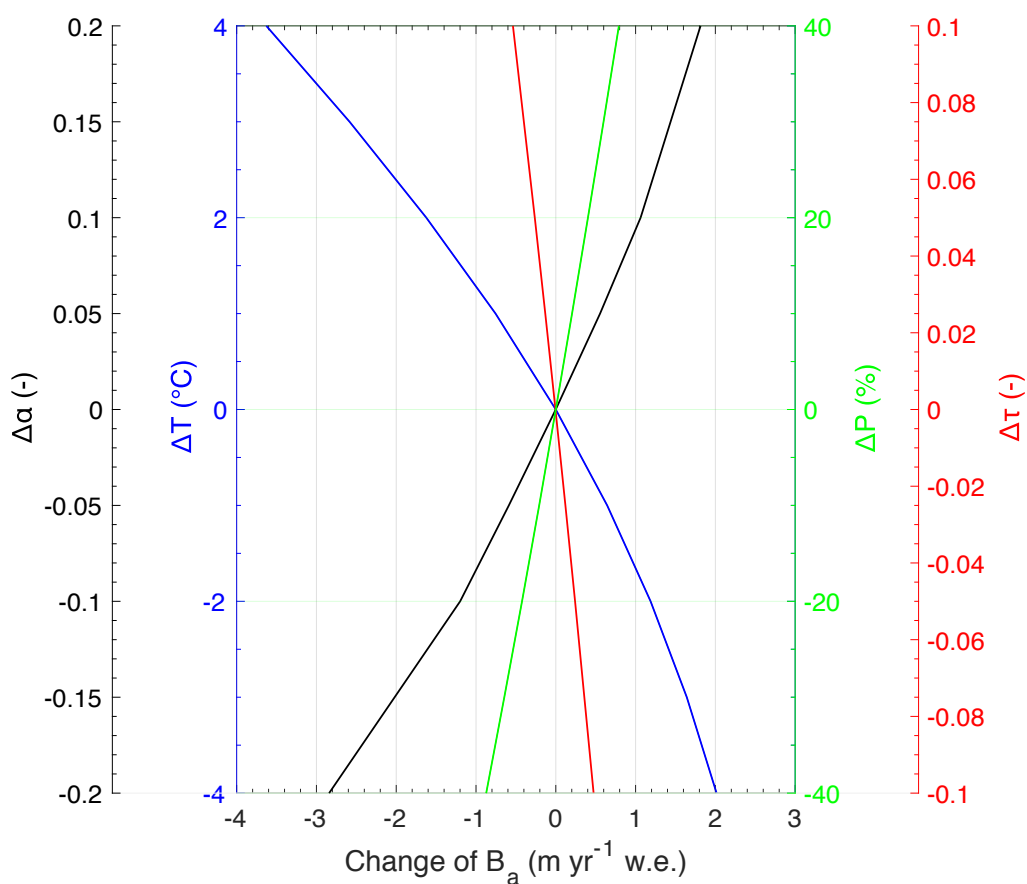
Figure 7. Modelled specific mass balance sensitivity of the Djankuat Glacier to changes in air temperature (ΔT), precipitation (ΔP), surface albedo (Δα) and atmospheric transmissivity (Δτ). All changes are relative to the 1967/68−2006/07 climatic conditions.

780

32
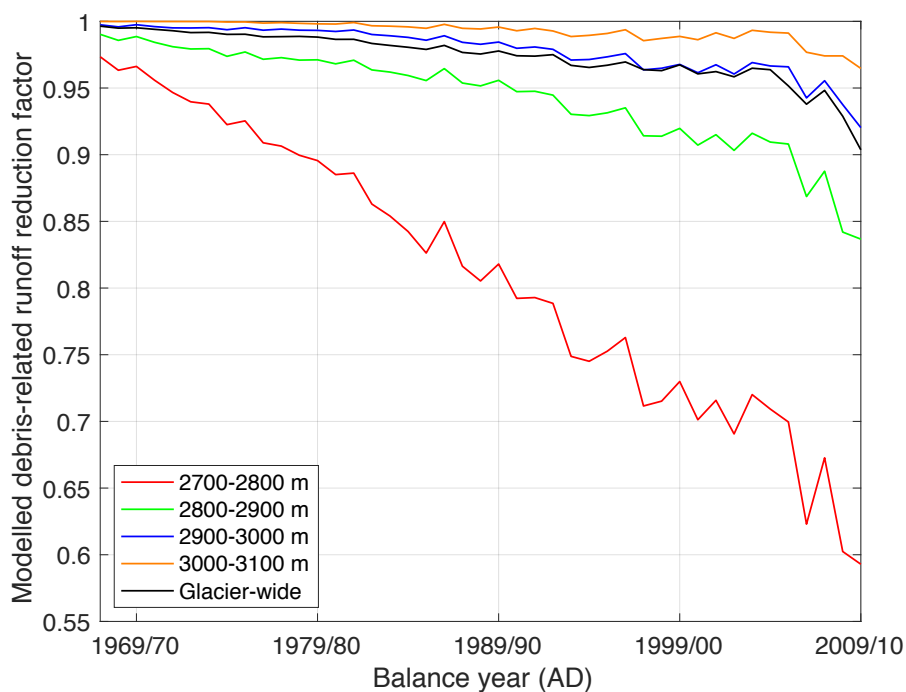
Figure 8. Modelled debris-related runoff reduction of the Djankuat Glacier in the 1967/68−2006/07 period, assuming fixed glacier geometry in the mass balance model. It must be noted that this value differs from what can be expected from the debris-related melt-reduction factor (f_{debris}) due to the inclusion of debris area (A_{debris}) and runoff from snow melt (W_{snow}) in the calculations.

785
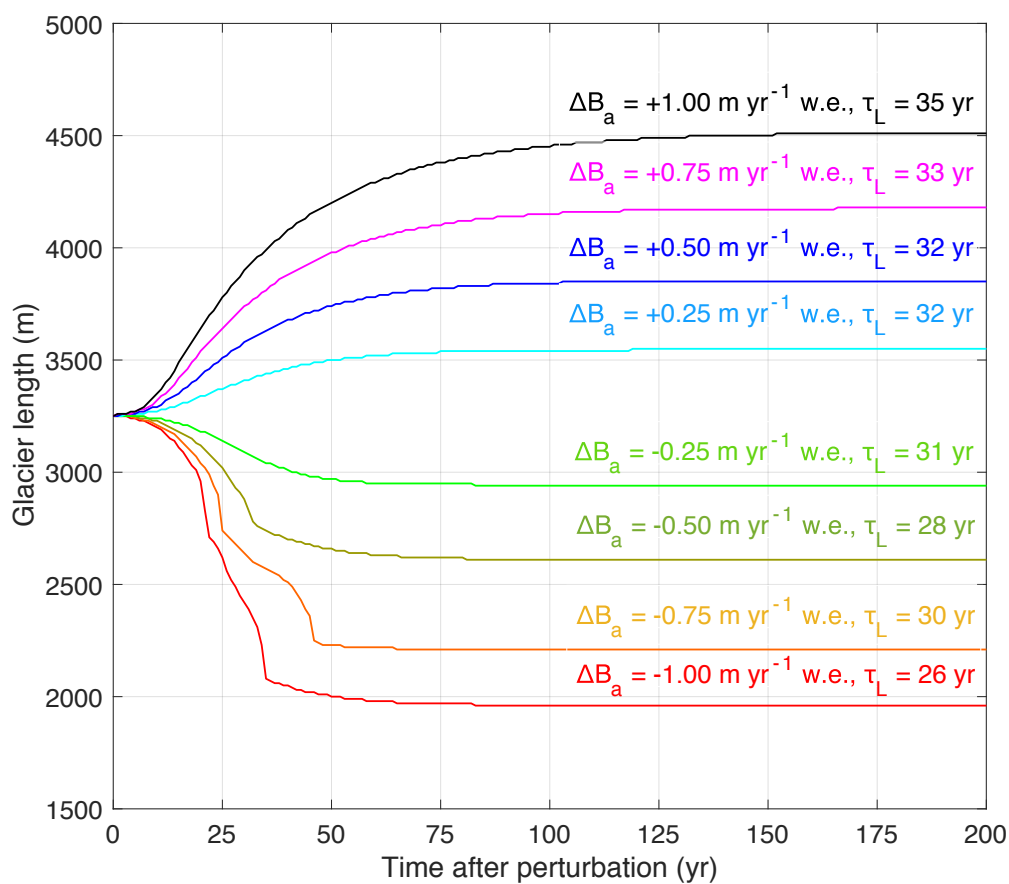
Figure 9. Sensitivity of the glacier steady state length L and e-folding length response time (τ_L) to mass balance perturbations ΔB_a with a varying magnitude.
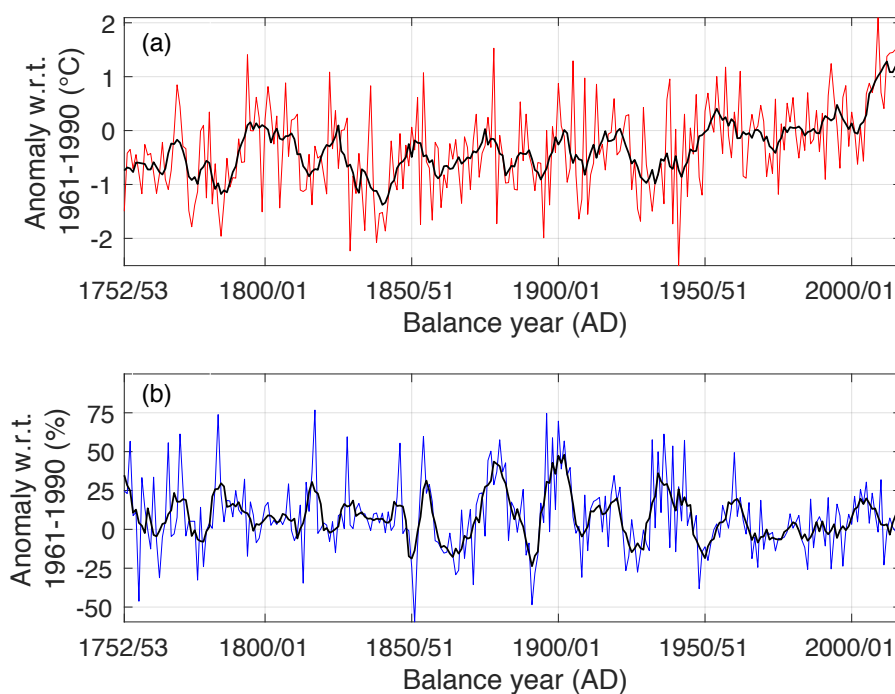
Figure 10. Reconstructed evolution of mean annual temperature and total precipitation amounts for Terskol weather station, based upon proxy data (tree ring reconstructions) and measurements from nearby weather stations (Mestia, Pyatigorsk and Mineralnye Vody). We refer to the text and Table 2 for more details.
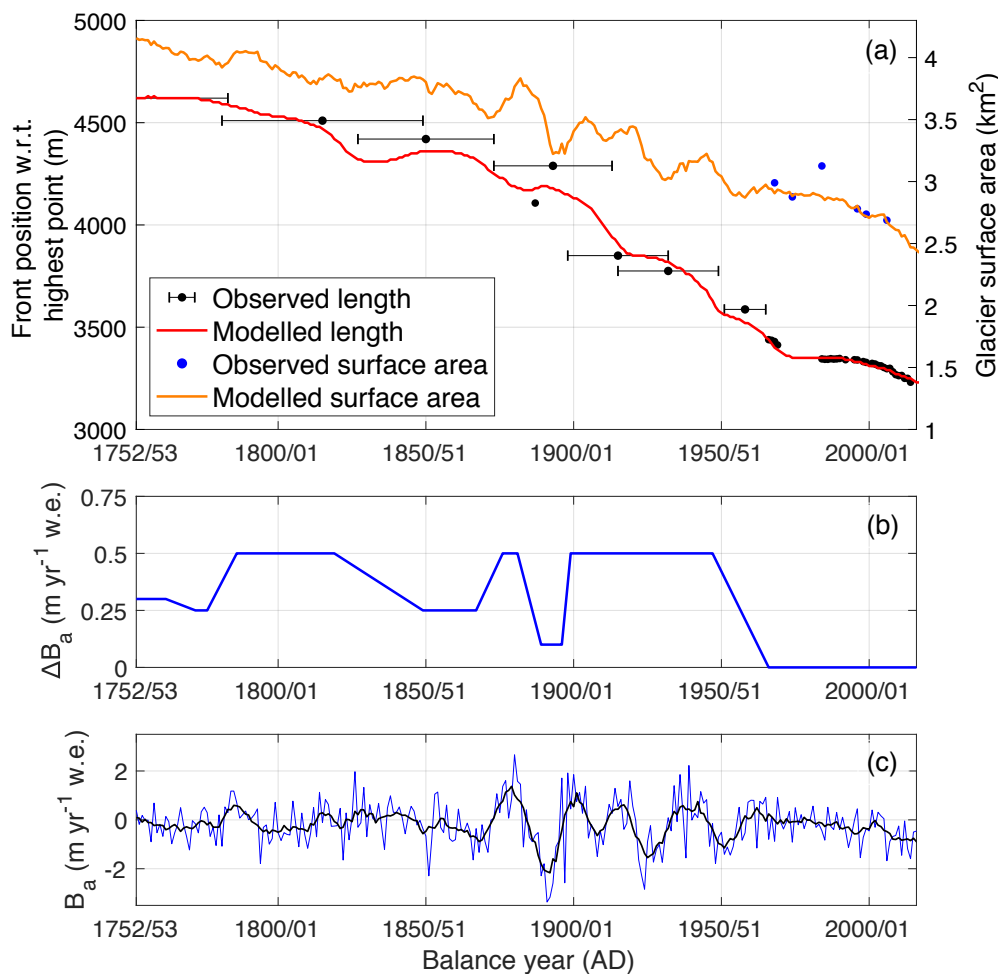
Figure 11. Historic variations of the (a) modelled and observed glacier length of the Djankuat Glacier since 1752/53 AD, (b) additional mass balance perturbations ΔB_a used in the dynamic calibration procedure and (c) reconstructed time series of the total annual mass balance B_a of the Djankuat Glacier with changing geometry. Observed length variations are derived from lichenometric dating of moraines in the paleovalley, historic documents and/or field measurements (Boyarsky, 1978; Zolotarev, 1998; Petrakov et al., 2012; WGMS, 2018).
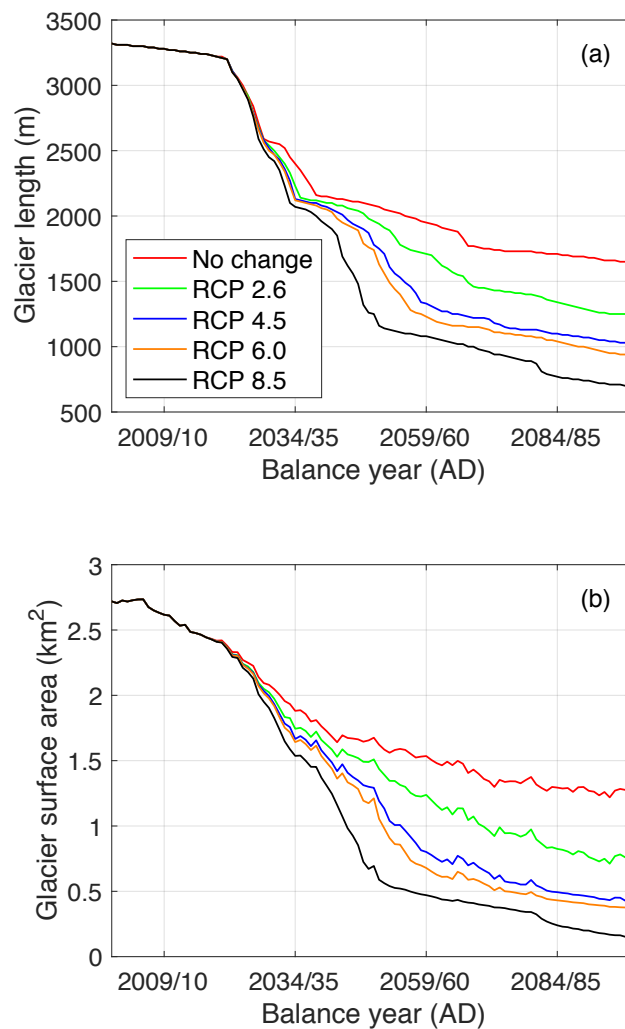
Figure 12. Modelled (a) glacier length and (b) glacier surface area of the Djankuat Glacier for different RCP scenarios until 2100 AD.
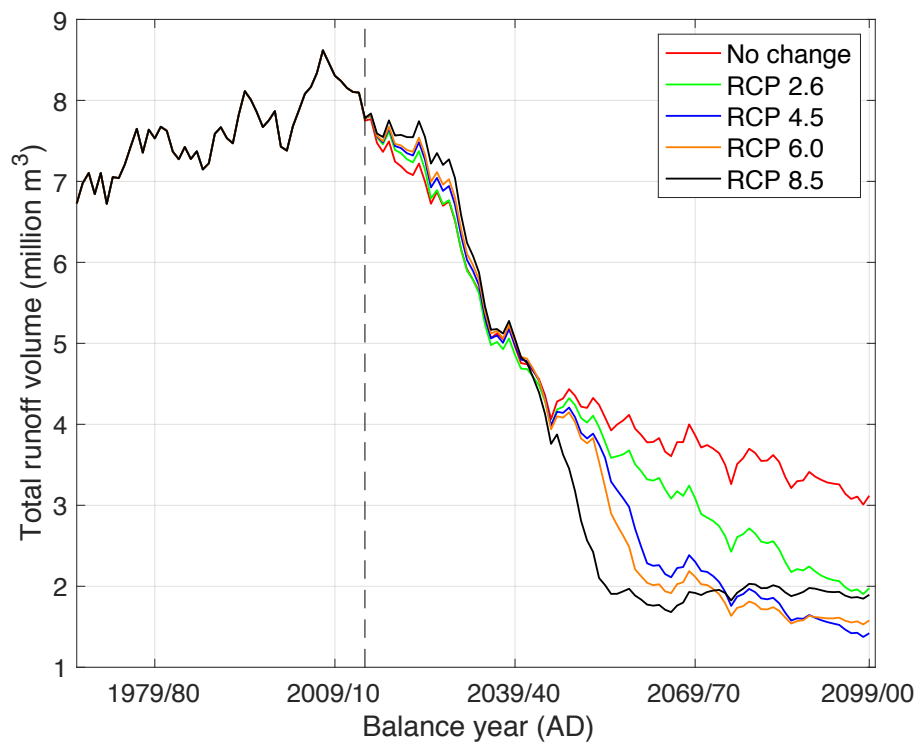
Figure 13. Simulated and projected 7-yr moving average of the total runoff volume of the Djankuat Glacier. The dashed
805   vertical line denotes the present (past to the left and future to the right).

Figure 14. Impact of debris input location x_{debris}, time of release of the debris source t_{debris} and debris flux magnitude F_{debris} (rows) on the future length extension of the Djankuat Glacier under different climatic scenarios (columns).

The Cryosphere
Discussions
Open Access

Table 1. Variables and their units used in the model.

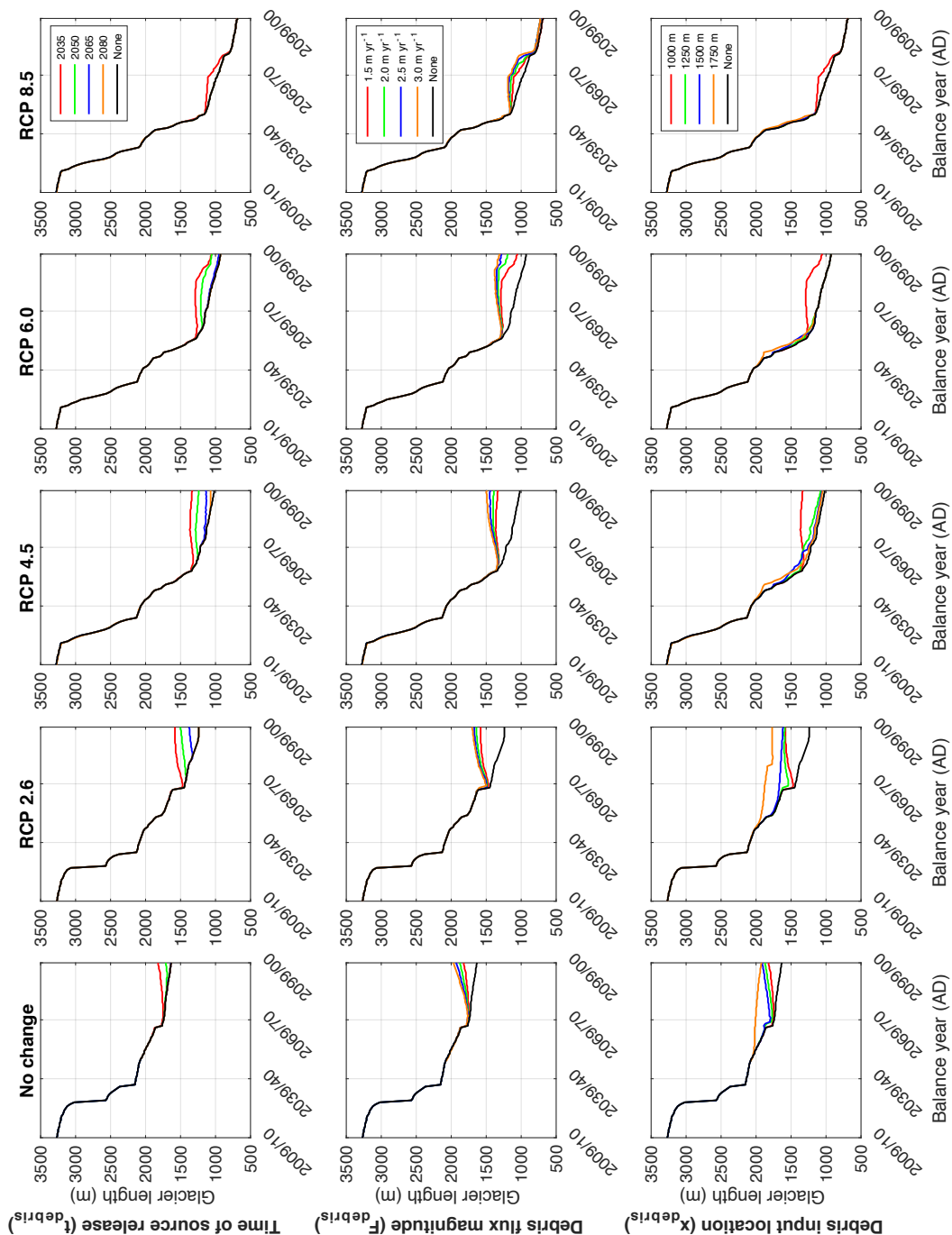| Variable	Symbol	Value	Unit	Variable	Symbol	Value	Unit
Supraglacial debris cover model							
Timestep debris model	Δt	0.01	a	Spatial resolution debris model	Δx	10	m
Characteristic debris thickness	H^*_{debris}	1.15	m	Debris melt-reduction factor	f_{debris}	-	-
Debris thickness	H_{debris}	-	m	Growth factor debris area	G_A	-	yr^{-1}
Debris-covered area	A_{debris}	-	km^2	Englacial debris concentration	C_{debris}	1.05	kg m^{-3}
Debris cover porosity	ϕ_{debris}	0.43	-	Debris rock density	ρ_{debris}	2600	kg m^{-3}
In/output of debris w.r.t. the glacier surface	I_{debris}	-	m yr^{-1}	Input flux to the glacier surface at input location	F^{input}_{debris}	1.60	m yr^{-1}
Debris input location	x_{debris}	1680	m	Deposition flux into the foreland	$F^{x=T+1}_{debris}$	-	m yr^{-1}
Foreland deposition rate of debris at terminus	$F^{x=T}_{debris}$	-	m yr^{-1}	Distance along flow line	x	-	m
Time of release of debris source	t_{debris}	1958	yr	Constant for strength of debris foreland deposition	c_T	1	m^{-1}
Distance to the front	D_T	-	m	Average debris thickness of first 30 grid points	H^{front}_{debris}	-	m
Mass balance model							
Timestep mass balance model	Δt	3	hours	Spatial resolution mass balance model	Δx	10	m
Surface elevation	h	-	m	Fraction of diffuse solar radiation	f_{dif}	0.50	-
Elevation of Terskol weather station	$h_{Terskol}$	2141	m	Fraction of direct solar radiation	f_{dir}	0.50	-
Elevation of AWS on Djankuat	h_{AWS}	2960	m	Angle of incidence	θ	-	°
Elevation of AWS in Adylsu Valley	h_{Adylsu}	2650	m	Solar elevation angle	θ_e	-	°
Horizontal precipitation enhancement between Terskol and Adylsu Valley	f_e	1.5	-	Solar zenith angle	θ_z	-	°
Snow redistribution factor	f_{red}	-	-	Fractional cloud cover	f_{cl}	-	-
Precipitation ratio between glacier and Adylsu Valley	P_{ratio}	-	m yr^{-1} w.e.	Solid precipitation	P_{solid}	-	m yr^{-1} w.e.
Surface slope	s	-	°	Snow depth	d_{snow}	-	m w.e.
Threshold air temperature for rain-snow distinction	T_{tresh}	2.0	°C	Incoming extra-terrestrial shortwave radiation at the TOA	$S_{\downarrow(TOA)}$	-	W m^2
Temperature lapse rate summer	$\gamma_{T(S)}$	-0.0067	$°\text{C m}^{-1}$	Characteristic snow depth	d^*_{snow}	0.011	m w.e.
Temperature lapse rate winter	$\gamma_{T(W)}$	-0.0049	$°\text{C m}^{-1}$	Outflow of retained melt water from snow	W_{snow}	-	m yr^{-1} w.e.
Precipitation lapse rate over glacier	γ_P	0.0023	$\text{m yr}^{-1}\text{ m}^{-1}$	Liquid snow store	w_{snow}	-	m w.e.
Net energy flux at glacier surface	Ψ_0	-	W m^2	Snowpack retention capacity	η_s	0.34	-
Albedo for ice	α_{ice}	0.22	-	Latent heat of fusion	L_m	334 000	J kg^{-1}
Albedo for snow	α_{snow}	0.79	-	Density of water	ρ_w	1 000	kg m^{-3}
Intercept $\Psi_0(\mathbf{T_{air}})$	c_0	-39.0	W m^{-2}	Threshold temperature $\Psi_0(\mathbf{T_{air}})$	T_{break}	0.0	°C
Slope $\Psi_0(\mathbf{T_{air}})$	c_1	13.0	$\text{W m}^{-2} °\text{C}^{-1}$	Atmospheric transmissivity	τ	0.53	-
Critical slope for loss due to redistribution	s_{crit}	25	°	Melt production from snow/ice	M	-	m yr^{-1} w.e.
Local annual (or specific) surface mass balance	b_a	-	m yr^{-1} w.e.	Total annual (or mean specific) mass balance	B_a	-	m yr^{-1} w.e.
Ice flow model							
Timestep flow model	Δt	0.0005	yr	Spatial resolution flow model	Δx	10	m
Distance along flowline (x-direction)	x	-	m	Ice thickness	H	-	m
Vertically averaged horizontal velocity	$\overline{u}$	-	m yr^{-1}	Surface elevation	h	-	m
Velocity related to internal deformation	$\overline{u}_d$	-	m yr^{-1}	Effective slope related to lateral valley wall angles	μ	-	-
Velocity related to basal sliding	u_s	-	m yr^{-1}	Ice density	ρ_i	917	kg m^{-3}
Surface velocity	u_{sfc}	-	m yr^{-1}	Gravitational acceleration	g	9.81	m s^{-2}
Ice volume flux	F_{ice}	-	$\text{m}^3\text{ yr}^{-1}$	Flow parameter related to internal deformation	f_d	$6.5 * 10^{-17}$	$\text{Pa}^{-3}\text{ yr}^{-1}$
Width (glacier surface)	W_{sfc}	-	m	Flow parameter related to basal sliding	f_s	$3.25 * 10^{-13}$	$\text{Pa}^{-3}\text{ m}^2\text{ yr}^{-1}$
Width (glacier bed)	W_0	-	m	Glacier length	L	-	m

810

40

Table 2. Input data used for the Terskol climatic reconstruction (1752−2100 AD).

Meteorological parameter	Source	Extent of dataset	Applied correction
Precipitation	Proxy data (D'Arrigo et al., 2001; Toucham et al., 2003; Akkemik et al., 2005; Akkemik & Aras, 2005; Griggs et al., 2007; Köse et al., 2011; Martin-Benito et al., 2016)	1752−…	(1) Average all datasets on a yearly basis (2) Match monthly amount and standard deviation with Terskol data series in the overlapping part of the datasets. (3) Convert to 3-hourly values by using the observed 1977−2013 Terskol data sequence as base, but corrected for monthly amounts derived before.
	Pyatigorsk weather station	1934−1997	
	Mestia weather station	1961−2010	
	Terskol weather station	1977−2013 (gap 1990−1997)	
	Mineralnye Vody weather station	1938−2018	
	CMIP5 simulations Georgia (Alder & Hostetler, 2013)	2018−2100	Linear change over the years until 2071−2095 mean amount matched output from RCP scenario
Temperature	Proxy data (Holobaca & Pop, 2015; Dolgova et al., 2017)	1752−…	(1) Average all datasets on a yearly basis (2) Match monthly amount and standard deviation with Terskol data series in the overlapping part of the datasets. (3) Convert to 3-hourly values by using the observed 1977−2013 Terskol data sequence as base, but corrected for monthly amounts derived before.
Temperature	CRUTEM4 dataset (Jones et al., 2012)	1850−2018	
Temperature	Mineralnye Vody weather station	1938−2018	
Temperature	Mestia weather station	1961−2010	
Temperature	Terskol weather station	1977−2013 (gap 1990−1997)	
Temperature	CMIP5 simulations Georgia (Alder & Hostetler, 2013)	2018−2100	Linear change over the years until 2071−2095 mean temperature matched output from RCP scenario

815   **Table 3.** Climatic scenarios for Terskol weather station in the future by the CMIP5 simulations (Alder and Hostetler, 2013).

Parameter	Reference climate (1967/68−2006/07)	No change (2071−2095)	RCP 2.6 (2071−2095)	RCP 4.5 (2071−2095)	RCP 6.0 (2071−2095)	RCP 8.5 (2071−2095)
Temperature (°C)	2.5	3.6 (+1.1)	4.0 (+1.5)	5.0 (+2.5)	5.5 (+3.0)	7.1 (+4.6)
Precipitation (mm yr⁻¹)	935.2	999.2 (+7 %)	857.8 (-8 %)	867.6 (-7 %)	887.1 (-5 %)	857.8 (-8 %)